RESEARCH ARTICLE SUMMARY

NEUROSCIENCE

Sexually dimorphic dopaminergic circuits determine sex preference

Anqi Wei†, Anran Zhao†, Chaowen Zheng†, Nan Dong†, Xu Cheng, Xueting Duan, Shuaijie Zhong, Xiaoying Liu, Jie Jian, Yuhao Qin, Yuxin Yang, Yuhao Gu, Bianbian Wang, Niki Gooya, Jingxiao Huo, Jingyu Yao, Weiwei Li, Kai Huang, Haiyao Liu, Fenghan Mao, Ruolin Wang, Mingjie Shao, Botao Wang, Yichi Zhang, Yang Chen, Qian Song, Rong Huang, Qiumin Qu, Chunxiang Zhang*, Xinjiang Kang*, Huadong Xu*, Changhe Wang*

INTRODUCTION: Innate social behaviors are essential for survival and reproduction. Animals should make correct social decisions (e.g., when, where, how, and with whom) to reach a maximal benefit from social interactions, especially when confronted with conflicts between innate requirements and external threats. However, how social decisions are convergently encoded by the internal-drive condition and external-environment context remains unclear. Furthermore, the sex of a social partner is a fundamental component affecting social decision-making. Interactions with individuals of the opposite sex are vital for the innate requirements of mating and reproduction, whereas same-sex social interaction provides social support and facilitates collaboration for shared goals. However, the neural mechanisms underlying sociosexual preference remain virtually unknown.

RATIONALE: We investigated the sociosexual preference of male and female mice under both normal conditions and when exposed to external threats. By using dual-color fiber photometry Ca^{2+} recordings and projection-specific chemogenetic and optogenetic manipulations of dopamine (DA) neurons in the ventral tegmental area (VTA), we defined the sexually dimorphic DA circuits responsible for the switching of sociosexual preferences.

RESULTS: Both male and female mice exhibited a preference for social interaction with females but shifted to male preference when facing survival threats mediated via different sensory pathways, such as olfaction [through testing with the stressor trimethylthiazoline (TMT)], vision (contextual fear conditioning), and auditory (cued fear conditioning), indicating the integrated encoding of social decisions in response to innate requirements and external environmental factors.

Using c-Fos staining and photometric Ca^{2+} recordings, we observed a strong correlation between the excitation of VTA^{DA} neurons and the switching of sexual preference when confronted with survival stress. Chemogenetic activation of VTA dopaminergic (VTA^{DA}) neurons facilitated male preference, whereas inhibiting these neurons blocked TMT's effects on the switching of sexual preference in both sexes, validating the critical role of VTA^{DA} neurons in orchestrating the shift in social preference.

Dual-color fiber photometry Ca^{2+} recordings and projection-specific chemogenetic manipulations demonstrated that sexually dimorphic alterations in VTA^{DA} circuits dictate the switching of sociosexual preference in response to external survival threats. The competition between two VTA^{DA} pathways, representing the balance between innate requirements and external threats, was used by males to encode their sexual preferences. VTA^{DA} projections to the nucleus accumbens (NAc) were predominant under normal conditions to promote female preference, whereas projection to the medial preoptic area (mPOA) mediated male preference in response to survival threats.

By contrast, firing-pattern alteration of the VTA^{DA}-NAc projection was utilized by females to determine their sexual preference. Female interactions were associated with stronger and faster Ca^{2+} transients, indicating the occurrence of phasic-like action potential (AP) firings of NAc-projecting VTA^{DA} neurons in female mice. On the other hand, male interactions facilitated by environmental threats were correlated with Ca^{2+} signals exhibiting slower kinetics, reflecting the sustained tonic-like AP firings of these neurons. Notably, the phasic firing–like optogenetic excitation of VTA^{DA}-NAc terminals resulted in larger transients of DA release, promoting female preference through the enhanced DA-D1R transmission (D1R, type 1 DA receptor). Conversely, the tonic firing–like excitation of these terminals induced a lower sustained DA release and thus led to male preference through the predominant DA-D2R transmission (D2R, type 2 DA receptor).

CONCLUSION: Both male and female mice exhibit female preference but shift to male preference when confronted with survival threats. The sexually dimorphic alterations in VTA^{DA} circuits, including neuronal activity, DA transmission, and circuit integration, play a key role in encoding the switch of sociosexual preference in both sexes. Our study thus introduces a neural mechanism for understanding how social decisions can be convergently determined by the balance between innate requirements and external survival threats. ■

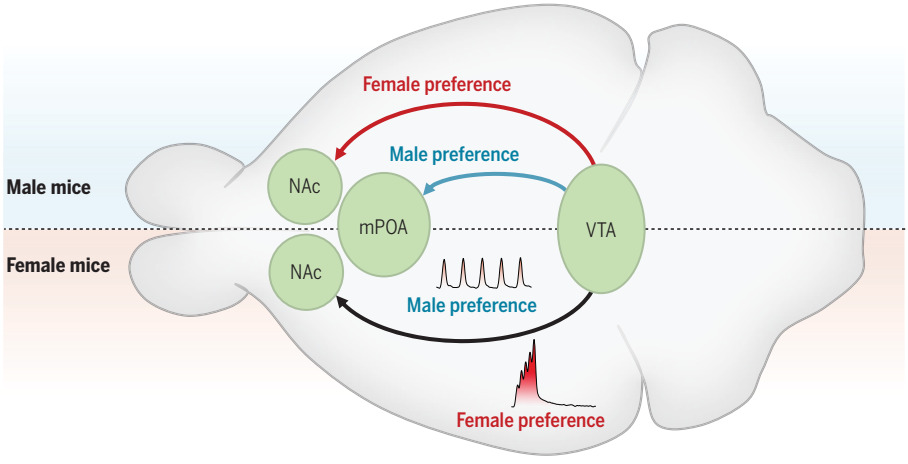

Sexually dimorphic dopamine circuits determine sociosexual preference. Male individuals use the competition between VTA^{DA}-NAc–projecting pathways (promoting female preference) and VTA^{DA}-mPOA–projecting pathways (promoting male preference upon survival stress) to determine their social decisions. Conversely, firing-pattern alteration of the VTA^{DA}-NAc projection is utilized by females to determine their sociosexual preferences, mediating female preference through the phasic firing–dominated DA-D1R transmission and male preference through the tonic firing–facilitated DA-D2R transmission when confronted with survival stress.

The list of author affiliations is available in the full article online.
*Corresponding author. Email: changhewang@xjtu.edu.cn (C.W.); hdxu@pku.edu.cn (H.X.); kxj335@163.com (X.K.); zhangchx999@163.com (C.Z.)
†These authors contributed equally to this work.
Cite this article as A. Wei *et al.*, *Science* **387**, eadq7001 (2025). DOI: 10.1126/science.adq7001

READ THE FULL ARTICLE AT
https://doi.org/10.1126/science.adq7001

RESEARCH ARTICLE

NEUROSCIENCE

Sexually dimorphic dopaminergic circuits determine sex preference

Anqi Wei[1]†, Anran Zhao[1]†, Chaowen Zheng[1]†, Nan Dong[1]†, Xu Cheng[2,3], Xueting Duan[1], Shuaijie Zhong[1], Xiaoying Liu[1], Jie Jian[2], Yuhao Qin[1], Yuxin Yang[1,4], Yuhao Gu[1], Bianbian Wang[1], Niki Gooya[5], Jingxiao Huo[1], Jingyu Yao[1], Weiwei Li[1,6], Kai Huang[1], Haiyao Liu[1], Fenghan Mao[1], Ruolin Wang[1], Mingjie Shao[1], Botao Wang[1], Yichi Zhang[1], Yang Chen[1], Qian Song[1], Rong Huang[1], Qiumin Qu[1], Chunxiang Zhang[2]*, Xinjiang Kang[2,3,4]*, Huadong Xu[1]*, Changhe Wang[1,2,3,7]*

Sociosexual preference is critical for reproduction and survival. However, neural mechanisms encoding social decisions on sex preference remain unclear. In this study, we show that both male and female mice exhibit female preference but shift to male preference when facing survival threats; their preference is mediated by the dimorphic changes in the excitability of ventral tegmental area dopaminergic (VTA^{DA}) neurons. In males, VTA^{DA} projections to the nucleus accumbens (NAc) mediate female preference, and those to the medial preoptic area mediate male preference. In females, firing-pattern (phasic-like versus tonic-like) alteration of the VTA^{DA}-NAc projection determines sociosexual preferences. These findings define VTA^{DA} neurons as a key node for social decision-making and reveal the sexually dimorphic DA circuit mechanisms underlying sociosexual preference.

Innate social behaviors, such as mating, consolation, and collaboration, are fundamental for reproduction, health, and survival, and provide adaptive benefits by offering greater capabilities for resource acquisition and defense against threats (*1*–*3*). Social decisions are dynamically adjusted to reach a maximal benefit from social engagement, particularly when confronted with conflicts between innate requirement and external threat (*4*–*11*). Multiple brain regions, including the ventral tegmental area (VTA) (*12*–*15*), medial prefrontal cortex (mPFC) (*16*–*18*), amygdala (*3*, *16*, *17*, *19*, *20*), nucleus accumbens (NAc) (*13*, *21*, *22*), dorsal raphe nucleus (*23*), insular cortex (*24*), and medial preoptic area (mPOA) (*19*, *25*, *26*), have been reported to be functionally involved in the modulation of social decision-making; however, how social decision-making is convergently encoded by the internal-drive condition and external-environment context remains largely unknown (*27*).

The selection of social encounters is one of the most fundamental components of social decision-making and involves consideration of sex, age, hierarchy, health, and other factors (*7*, *28*). Social interaction with individuals of the opposite sex, especially in the context of mating and procreation, is crucial for the innate requirements of reproduction and genetic continuity across generations (*29*, *30*). Concurrently, same-sex social networks often serve as a source of protection and social support that are vital for health and survival, and these social engagements can facilitate coordination and collaboration for shared goals (*31*, *32*). However, the neural mechanisms through which sociosexual preference (social preference to male or female conspecifics) can be determined—and how this preference is modulated by the external environment—remain virtually unknown.

Switching of sociosexual preference under survival stress

To investigate whether and how the sociosexual preference can be altered in the context of survival threats, we conducted a three-chamber social interaction assay to assess sex preference in the absence or presence of trimethylthiazoline (TMT), a potent stressful odor cue linked with survival threats for rodents (*33*, *34*). Consistent with a previous report (*33*), male mice displayed a pronounced preference for female mice (Fig. 1A and fig. S1A), which conforms to the innate requirements in mating and reproduction. This preference was dramatically reversed upon exposure to the TMT stressor, shown as a decrease in the time interacting with female mice and an increased visiting time with male mice (Fig. 1A and fig. S1A). Consequently, the proportion of time allocated to male interaction increased from ~34% under control conditions to ~56% when they were exposed to TMT (Fig. 1A). In parallel with this behavioral shift, the female-bedding preference for male mice was also reversed in the presence of TMT (Fig. 1B and fig. S1B). To confirm that the enhanced male interaction was due to preference alteration between different sexes rather than an aversion to females under TMT conditions, we conducted similar behavior tests to compare the preference for a conspecific partner versus a toy mouse. We found that male mice showed a clear preference for conspecific partners, regardless of the sex of the social partner, and this preference was further increased by the exposure to the TMT stressor (fig. S1, C and D), supporting the idea that male mice switch to male preference when confronted with TMT exposure. This phenomenon suggests that the environmental context exerts a strong impact on social preferences and underscores the dynamic nature of sociosexual preference in response to innate requirements and external survival threats.

To ascertain that the observed changes in social preference were attributable to the social context of survival stress rather than the specific odorant stimulation, we carried out a fear conditioning (FC) test associated with visual and auditory cues and assessed the sex preference of male mice (Fig. 1C). Consistently, male mice also exhibited female social preference under the control condition with no electric shock during the preconditioning procedure (Fig. 1D and fig. S1E). By contrast, when subjected to the visual contextual FC conditions, the preconditioned male mice allocated more time to interacting with male mice (Fig. 1D). Similarly, in male animals, the preference for female mice was also switched to male preference in auditory-cued FC tests (Fig. 1E and fig. S1F). These results suggest that the sociosexual preference of male mice can be modulated by survival stress through various sensory pathways such as olfaction (TMT), vision (contextual FC), or auditory (cued FC).

We next investigated the social preference of female mice when exposed to survival stressors. Female mice also showed preference for female encounters under control conditions (Fig. 1F and fig. S1G). However, TMT exposure increased the interaction time with male mice and reduced the time spent with female counterparts (Fig. 1F and fig. S1G). Consequently, the proportion of social time that female mice spent with males increased substantially in the presence of TMT (Fig. 1F). Similarly, the female-bedding preference of female mice was also reversed to male-bedding preference upon TMT exposure (Fig. 1G and fig. S1H). Such changes were not

[1]Department of Neurology, the First Affiliated Hospital, Neuroscience Research Center, Key Laboratory of Biomedical Information Engineering of Ministry of Education, School of Life Science and Technology, Xi'an Jiaotong University, Xi'an, China. [2]Key Laboratory of Medical Electrophysiology, Ministry of Education of China, Collaborative Innovation Center for Prevention and Treatment of Cardiovascular Disease, and the Institute of Cardiovascular Research, Southwest Medical University, Luzhou, Sichuan, China. [3]Department of Neurosurgery, the Affiliated Hospital of Southwest Medical University, Luzhou, Sichuan, China. [4]College of Agriculture and Biology, Liaocheng University, Liaocheng, China. [5]Solomon H. Snyder Department of Neuroscience, Johns Hopkins University School of Medicine, Baltimore, MD, USA. [6]Department of Acupuncture, Massage and Rehabilitation, Shaanxi Provincial Hospital of Chinese Medicine, Xi'an, China. [7]Department of Neurology, the Second Affiliated Hospital of Xi'an Jiaotong University, Xi'an, China.
***Corresponding author. Email: changhewang@xjtu.edu.cn (C.W.); hdxu@pku.edu.cn (H.X.); kxj335@163.com (X.K.); zhangchx999@163.com (C.Z.)**
†These authors contributed equally to this work.

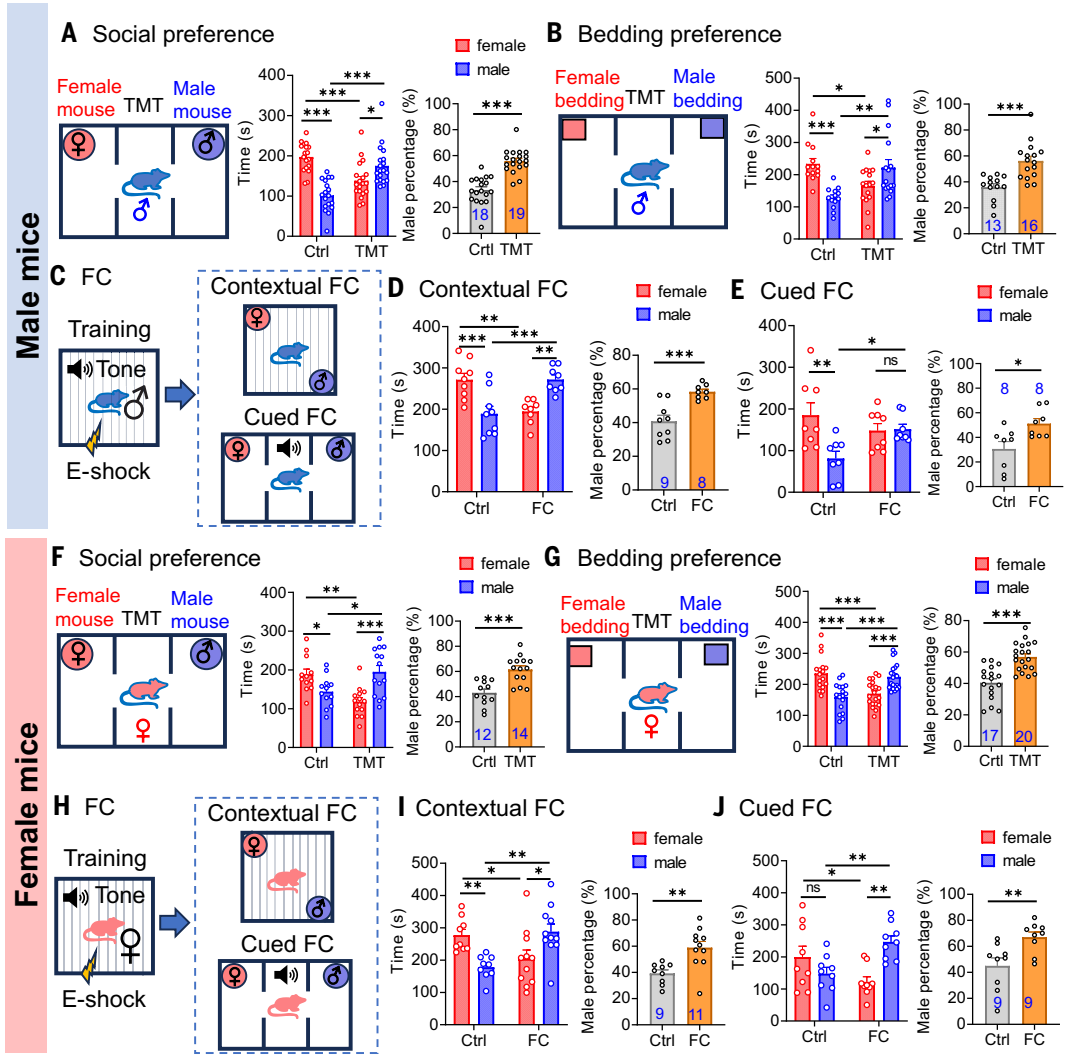

Fig. 1. Sexually dimorphic changes of sociosexual preference under survival stress. (**A**) (Left) Schematic diagram showing the social preference test, and (right) statistics of social interaction time for female or male encounters and percentage of male-interaction time of male mice in the absence [control (Ctrl)] or presence (TMT) of the stressor TMT. (**B**) Similar to (A), except that bedding preference test was performed. (**C**) Schematic of acquisition and extinction of conditioned fear (FC) through contextual or tone-based conditioning. (**D** and **E**) Statistics of social time (left) and male social percentage (right) in contextual (D) and cued (E) FC tests. (**F** to **J**) As shown in (A) to (E), except that female mice were used. Data are presented as mean ± SEM. Two-way analysis of variance (ANOVA) for comparison of time spent on male and female mice between Ctrl and TMT groups; unpaired Student's *t* test for male percentage. $^{*}P < 0.05$, $^{**}P < 0.01$, $^{***}P < 0.001$.

due to an aversion to females, because TMT exposure also increased the social preference of female mice for female partners compared with toy mice (fig. S1, I and J). Furthermore, fear-conditioned female mice spent more time with male mice and less time with female ones, as compared with the control group that did not receive shock conditioning, in both the contextual and cued FC tests (Fig. 1, H to J, and fig. S1, K and L). Collectively, these results provide compelling evidence that both males and females shift their social preference toward male interactions when confronted with survival stressors.

VTA^{DA} neuron is essential for the switching of sociosexual preference

Where and how is the sociosexual preference encoded in the brain? The mesolimbic dopamine (DA) pathway originating from the VTA has been implicated in both social interaction (*34*–*36*) and sexual motivation (*21*, *37*–*39*). This pathway is activated when individuals experience incentives (both positive and negative), rewards, or the anticipation of rewards from social engagements (*14*, *40*, *41*). Moreover, DA release exhibits sexual dimorphism during mating and aggressive behaviors (*21*), suggesting a potential role in modulating sociosexual preferences. Therefore, we next investigated whether and how mesolimbic DA pathways are functionally involved in the threat-induced shifts in male preference by using c-Fos expression as a biomarker of neural activity. As anticipated, both male and female mice spent more time approaching and interacting with the caged stranger male mice when exposed to TMT (Fig. 2, A and E, and fig. S2, A and D). Concurrently, the number of c-Fos expressing neurons increased greatly in the VTA in both sexes (Fig. 2, B, D, F, and H), indicating the increased neural activity in this region upon TMT exposure. Immunostaining analysis showed that most of c-Fos positive neurons (~84.6% in males and ~82.6% in females) colocalized with tyrosine hydroxylase (TH), a specific molecular marker for DA neurons (fig. S2, C and F). These findings indicate that dopaminergic neurons in the VTA (VTA^{DA} neurons) may play a crucial role in the modulation of sex preference during social interaction in both male and female animals. In male mice exposed to TMT during social interaction, there was also a pronounced increase of c-Fos expression in the mPOA (Fig. 2, C and D), a downstream brain region of VTA^{DA} neurons implicated in mating, parental support, and defensive and aggressive behaviors (*42*–*48*). This increase was not observed in other DA downstream regions, such as the NAc, mPFC, or basolateral amygdala (BLA) (Fig. 2, C and D, and fig. S2B). By contrast, in female animals that were exposed to TMT during social activities, the increase of c-Fos expression was specifically observed in the NAc, a central hub in the DA reward system (*49*, *50*), but not in the mPOA, mPFC, or BLA (Fig. 2, G and H, and fig. S2E). Specifically, the increased c-Fos staining was mainly located in the core region of the NAc, although both the core and the shell regions are relevant to social reward and social interaction (*21*, *51*). These sexually dimorphic changes in

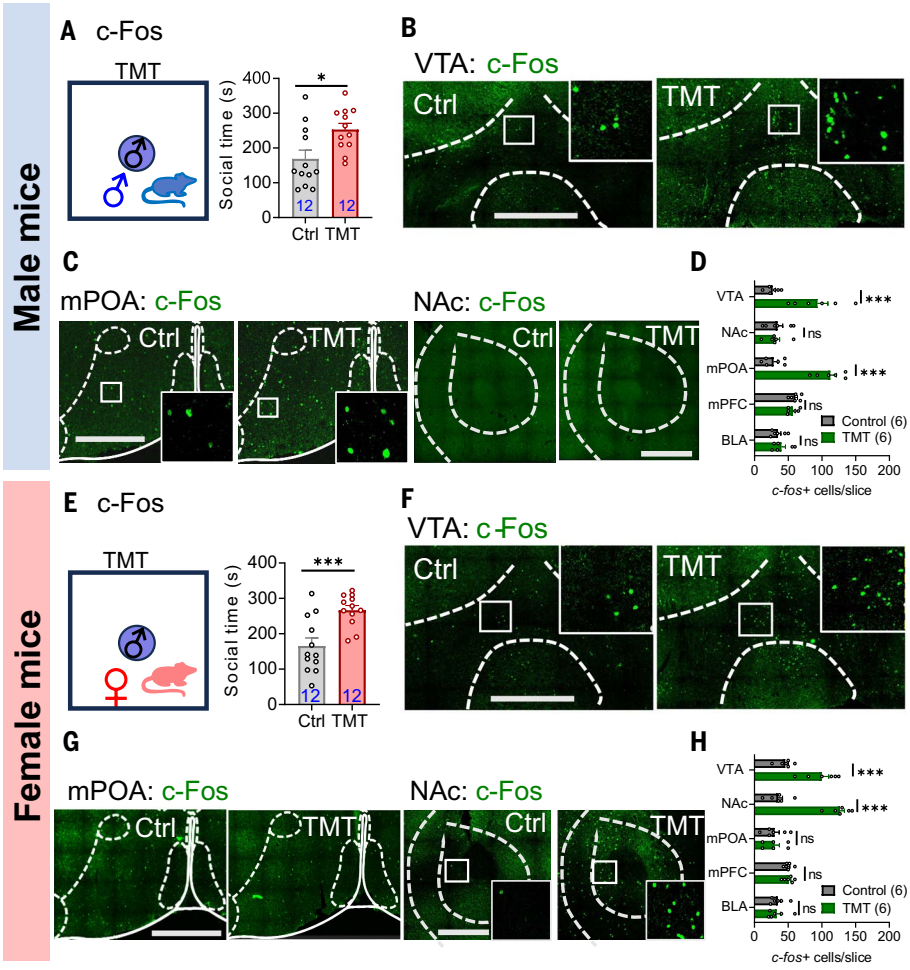

Fig. 2. Sexually dimorphic changes of DA system under survival stress. (**A**) (Left) Schematic showing the open-field social test, and (right) statistics of social interaction time of male mice in the absence (Ctrl) or presence of TMT. (**B** to **D**) Representative micrographs, and statistics of c-Fos–positive neurons in the VTA, NAc, mPOA, mPFC, and BLA from animals as shown in (A). Scale bars, 500 μm. (**E** to **H**) As shown in (A) to (D), except that female mice were used. Scale bars, 500 μm. Data are presented as mean ± SEM. Unpaired Student's *t* test for social time for (A) and (E) and c-Fos staining for (D) and (H). ns (not significant), $P > 0.05$; *$P < 0.05$; ***$P < 0.001$.

c-Fos expression patterns in response to TMT exposure suggest that the mesolimbic DA pathways may be differentially involved in the modulation of sociosexual preference under survival threats in both sexes.

To substantiate the functional changes of VTA^{DA} neurons, we injected TH-Cre and Cre-dependent GCaMP (a genetically encoded Ca^{2+} indicator)–expressing viruses into the VTA of male mice for the specific expression of GCaMP in VTA^{DA} neurons. Fiber photometry recording of Ca^{2+} signals was conducted to monitor the activity of VTA^{DA} neurons during an open-field social interaction test involving mouse partners of both sexes (Fig. 3, A and F, and fig. S3, A and B). Interactions with either sex of mice induced Ca^{2+} transients in VTA^{DA} neurons of male mice. In general, interaction with female animals provoked a more pronounced Ca^{2+} signal compared with that elicited by male interactions (Fig. 3B and fig. S3, C and D). However, repeated socialization with the same mouse led to a decrease in Ca^{2+} signals (fig. S3, C and D). Along with the reversal of sex preference, the male interaction–coupled Ca^{2+} signals in male mice increased greatly in the presence of TMT in the testing apparatus, exhibiting larger amplitude and area under the curve (AUC) values than those under control conditions (Fig. 3, C to E).

We next performed similar experiments with female mice (Fig. 3F and fig. S3, E and F). Female interactions elicited stronger Ca^{2+} signals in VTA^{DA} neurons in female mice than those coupled with male interactions, although repeated socialization with the same sex led to a substantial decrease in Ca^{2+} signals (fig. S3, G and H). However, the larger Ca^{2+} signals during female interactions were substantially reversed by TMT exposure (Fig. 3, G and H). Both the amplitude and AUC values of Ca^{2+} signals triggered by male interactions were higher than those coupled to female interactions in the presence of TMT stressor (Fig. 3, I and J). These results suggest the critical involvement of VTA^{DA} neurons in shaping sociosexual preference of both sexes and indicate that the hyperactivity of VTA^{DA} neurons may be functionally involved in driving the preference shifts under conditions of survival stress.

To confirm the critical roles of VTA^{DA} neurons in male preference under TMT threat, TH-Cre and Cre-dependent hM3Dq-expressing viruses (with the Cre-dependent mCherry-expressing virus as a control) were stereotaxically coinjected into the VTA of male mice (Fig. 4A and fig. S4, A and B) for the chemogenetic manipulation of VTA^{DA} neurons. Compared with the control group, chemogenetic activation (hM3Dq) of VTA^{DA} neurons through the intraperitoneal (i.p.) injection (0.5 mg/kg) of clozapine *N*-oxide (CNO) increased the social time of male mice with male counterparts and reduced that with females, thereby resulting in male social preference (Fig. 4B and fig. S4C). Consistent with this, the chemogenetic activation group spent more time in male bedding and less time in female bedding (Fig. 4C and fig. S4D). In female mice, chemogenetic activation of VTA^{DA} neurons also led to an increase in social interaction with male mice and a pronounced reduction in interaction with female mice (Fig. 4, D and E, and fig. S4, E to G), as well as similar bedding preferences (Fig. 4F and fig. S4H). To achieve a more specific genetic manipulation of VTA^{DA} neurons, we conducted similar experiments by using DAT-Cre transgenic mice (fig. S5, A and E) instead of the coinjection with the TH-Cre virus (*52*). Similarly, chemogenetic activation of VTA^{DA} neurons through the i.p. injection of CNO switched the social preference from females to male in both sexes, whereas saline administration had no effect on social preference (fig. S5, B to D, and F to H). Concurrently, chemogenetic inhibition of VTA^{DA} neurons in both male and female DAT-Cre mice abolished their male preference in the presence of TMT stressor (fig. S6). Collectively, these results validate the critical roles of VTA^{DA} neurons in mediating the switching of social preference in both sexes.

Competition between VTA^{DA}-mPOA and VTA^{DA}-NAc projections dictates the sociosexual preference of male mice

Given that both female and male social interactions induced the hyperactivity of VTA^{DA} neurons in both sexes (Fig. 3) and that TMT exposure led to male preference accompanied by distinct c-Fos expression patterns in downstream brain regions (Fig. 2), we hypothesized that sexually dimorphic alterations in DA circuits might be responsible for the shift in sex

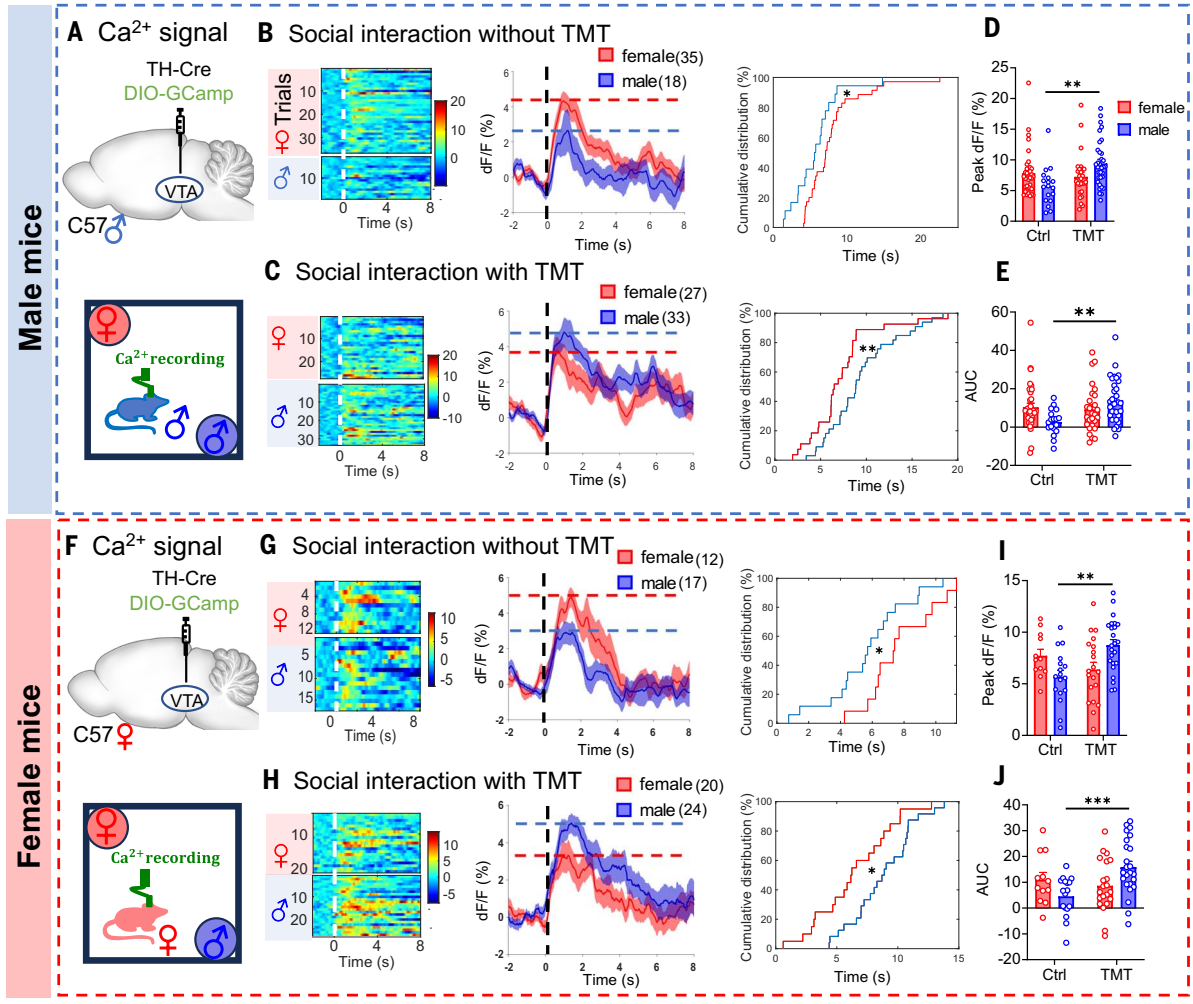

Fig. 3. Association of VTA^{DA} neural activity with the switching of sociosexual preference. (**A** to **E**) Schematic, heatmaps, averaged traces, and statistics of photometric Ca^{2+} recordings of VTA^{DA} neurons of male mice during social interactions in the absence or presence of TMT. (**F** to **J**) As shown in (A) to (E), except that female mice were used. Data are presented as mean ± SEM. Two-way ANOVA for (D), (E), (I), and (J); Kolmogorov-Smirnov test for peak distribution analysis of Ca^{2+} signals in (B), (C), (G), and (H). *P < 0.05, **P < 0.01, ***P < 0.001.

preference triggered by survival threats. Thus, we next investigated whether and how the VTA^{DA}-NAc (*53*, *54*) and VTA^{DA}-mPOA (*42*) pathways are involved. Double retrograde-virus tracing strategy was used to separately label VTA^{DA} neurons [blue fluorescent protein (BFP)] projecting to the NAc core and those [green fluorescent protein (GFP)] projecting to the mPOA (Fig. 5A and fig. S7, A and B). As expected, the retrograde viruses from the NAc (BFP) and the mPOA (GFP) mostly colocalized with TH (Fig. 5A). However, there was minimal colocalization between the two retrograde viruses (Fig. 5A), suggesting that the NAc-projecting and mPOA-projecting VTA^{DA} neurons represent distinct subpopulations.

To further investigate how the two DA circuits (VTA^{DA}→mPOA and VTA^{DA}→NAc) are functionally involved in the switching of sex preference in the context of survival threats, a retrograde-tracing viral vector expressing the red protein calcium indicator (jRGECO1) was injected into the NAc core, whereas a viral vector carrying the GCaMP was injected in the mPOA of male mice (Fig. 5B and fig. S7C). Dual-color fiber photometry recordings of jRGECO1 and GCaMP were conducted to simultaneously monitor Ca^{2+} signals in these two subpopulations of VTA^{DA} neurons (Fig. 5B). We found that the mPOA-projecting VTA^{DA} neurons exhibited a stronger response to male interactions, which was further strengthened in the presence of TMT. Both the peak and AUC values of the male interaction–coupled Ca^{2+} signals in mPOA-projecting VTA^{DA} neurons showed a substantial increase in the TMT context (Fig. 5, C to G). Although DA projections from the hypothalamus to the mPOA have been reported to be involved in male-female mating behaviors (*44*), the mPOA-projecting VTA^{DA} neurons showed only a minimal response to female interaction either under control conditions or after TMT exposure (Fig. 5, C to G). By contrast, the NAc-projecting VTA^{DA} neurons were only responsive to female interaction, which was markedly suppressed by TMT exposure (Fig. 5, C, and H to K). This is consistent with the finding that only a slight DA signal can be observed in the NAc during male-male social approach that is not followed by attacking or mounting (*21*). These findings suggest that the VTA^{DA}-mPOA projection is associated with male social preference, potentially being activated under conditions of survival threats. Conversely, the VTA^{DA}-NAc projection appears to underlie female preference in male mice, which is attenuated by the presence of survival stressors.

On the basis of these observations, we proposed that the balance between the VTA^{DA}-mPOA and VTA^{DA}-NAc projections determines the sex preference of male individuals during social interactions. To test this hypothesis, we next evaluated the mPOA dominance index, calculated using the formula $D = (F_{mPOA} - F_{NAc})/(F_{mPOA} + F_{NAc}) \times 100\%$, where F represents the

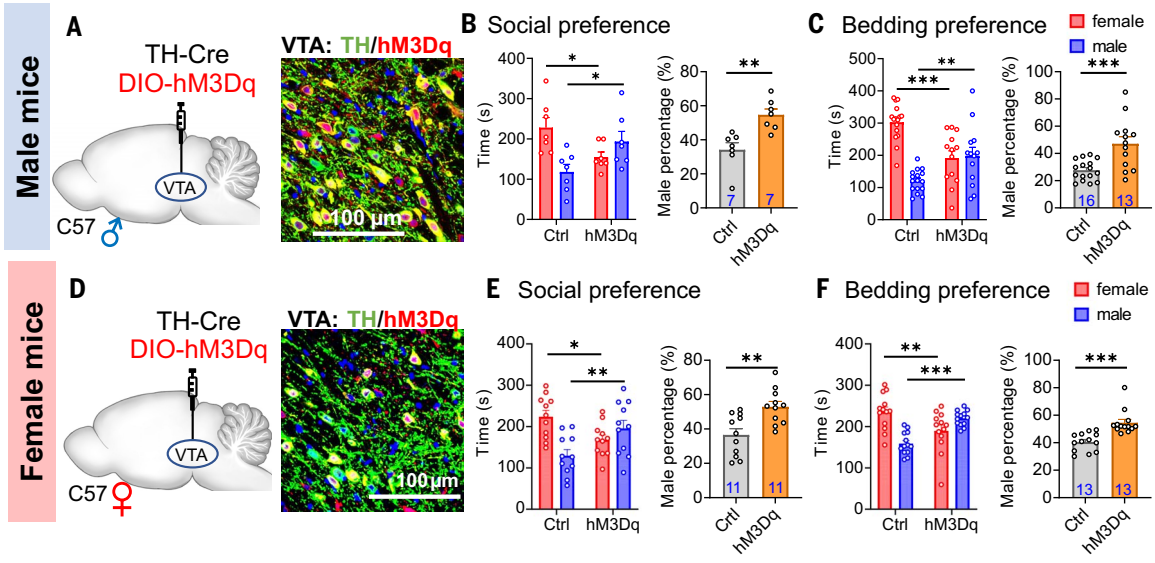

Fig. 4. VTA^{DA} neuron excitation facilitates male preference in both sexes. (**A** to **C**) Schematic of virus injection, representative micrograph showing the colocalization of mCherry and TH-staining in the VTA, and statistics of social preference and bedding preference tests after the chemogenetic activation of VTA^{DA} neurons. Scale bar, 100 μm. (**D** to **F**) As shown in (A) to (C), except that female mice were used. Data are presented as mean ± SEM. Two-way ANOVA for comparison of time spent on male and female mice between Ctrl and TMT group; unpaired Student's *t*-test for male percentage. **P* < 0.05, ***P* < 0.01, ****P* < 0.001.

normalized Ca^{2+} signal ($\Delta F/F_0$) as recorded above. When the mPOA dominance index was plotted against the interaction time with either males or females, we found a positive correlation with male-interaction time and a negative correlation with female-interaction time (Fig. 5L). The fitted lines intersected near the equilibrium point between the two projections (Fig. 5L), confirming our hypothesis that the confrontation between mPOA and NAc projections likely dictates the sex preference in male mice. For detailed analysis, we further divided the plots into two functional zones, in which the NAc projection was dominant in zone I and the mPOA projection was dominant in zone II (Fig. 5M). Consistent with the notion that TMT exposure enhances the activity of mPOA-projecting VTA^{DA} neurons, social interaction events under TMT exposure were predominantly distributed in zone II (Fig. 5, M and N). Male-interaction events under control conditions were evenly distributed but shifted predominantly to zone II upon TMT exposure (Fig. 5M). By contrast, female-interaction events were primarily found in zone I but also switched to zone II in the presence of TMT (Fig. 5M). Overall, male interactions were predominant in zone II, whereas female-interaction events were dominant in zone I (Fig. 5, N and O). The social time with males was much shorter than that with females in zone I, but this was reversed in zone II (Fig. 5, M and P), further confirming the correlation between the two DA neuron populations and sex preferences. Collectively, these findings strongly support the concept that the balance between VTA^{DA}-mPOA and VTA^{DA}-NAc projections is a pivotal determinant of sex preference in male individuals, especially when they are confronted with conflicts between innate requirements and external threats.

To further confirm the sexually dimorphic functions of the DA circuits in sex preference, TH-Cre and Cre-dependent hM3Dq-expressing viral vectors were coinjected into the VTA, and a cannula was implanted in the mPOA for the local application of CNO (Fig. 6A and fig. S8A). We found that chemogenetic activation of VTA^{DA} terminals in the mPOA increased the social time of male mice with males and decreased social time spent with females (Fig. 6B and fig. S8B), resulting in the pronounced shift in social preference from female to male encounters (Fig. 6B). Similar results were also observed in the bedding preference tests (Fig. 6C). Consistently, the TMT-induced male preference of male mice was diminished upon the chemogenetic inhibition of VTA^{DA} terminals in the mPOA (Fig. 6, D to F, and fig. S8, C and D). These results demonstrate the critical roles of VTA^{DA}-mPOA transmission in mediating the social preference for male conspecifics in male mice. By contrast, chemogenetic inhibition of VTA^{DA}-NAc core transmission led to the shift of social preference from female to male, whereas chemogenetic activation of this pathway reversed the male preference to females in male animals in the presence of TMT (Fig. 6, G to L, and fig. S9). These results show that the dynamic interplay between the VTA^{DA}-NAc and VTA^{DA}-mPOA pathways, representing the ongoing balance between innate requirements and external threats, determines the sociosexual preference of male mice.

Association of VTA^{DA}-NAc projection with the sociosexual preference of females

We next investigated neural mechanisms underlying the social preference of female mice with dual retrograde-tracing strategies. Similarly to what we observed in male mice, the retrograde viruses from the NAc (BFP) and the mPOA (GFP) both colocalized with TH in the VTA but showed minimal colocalization between BFP and GFP (fig. S10A), validating the distinct subpopulations of VTA^{DA} neurons that project to the NAc and the mPOA. To verify the functional roles of each DA projection in the sex preference of female mice, retrograde-tracing viral vectors expressing jRGECO1 and GCaMP were injected into the NAc and the mPOA, respectively, followed by dual Ca^{2+} recordings in the VTA (Fig. 7A and fig. S10B). Differently from what we observed in male mice, mPOA-projecting VTA^{DA} neurons in female mice showed no response to male interactions, irrespective of whether TMT was absent or present (Fig. 7, B to E, and fig. S10C). By contrast, NAc-projecting VTA^{DA} neurons displayed higher Ca^{2+} signals during social interactions with females, and this was reversed in the presence of TMT (Fig. 7, B, and F to H). Specifically, the amplitudes and AUC values of the Ca^{2+} signals during female interaction decreased, whereas those during male interaction increased greatly upon TMT exposure (Fig. 7, F to H, and fig. S10, D and E). Both female and male interactions correlated positively with the Ca^{2+} signals of NAc-projecting VTA^{DA} neurons. However, TMT exposure resulted in an opposite distribution of these social interaction events (Fig. 7, I and J). To quantify these changes, the distribution region was bifurcated into zone I and zone II by using the median percentile line of Ca^{2+} signals ($\Delta F/F_0$). Same-sex interaction events of female mice mainly localized in zone II with larger $\Delta F/F_0$ values and social interaction time under control conditions, whereas these same-sex social events were predominantly situated in zone I in the context of TMT (Fig. 7I). By contrast, opposite-sex interaction events were primarily localized in zone I and shifted to zone II

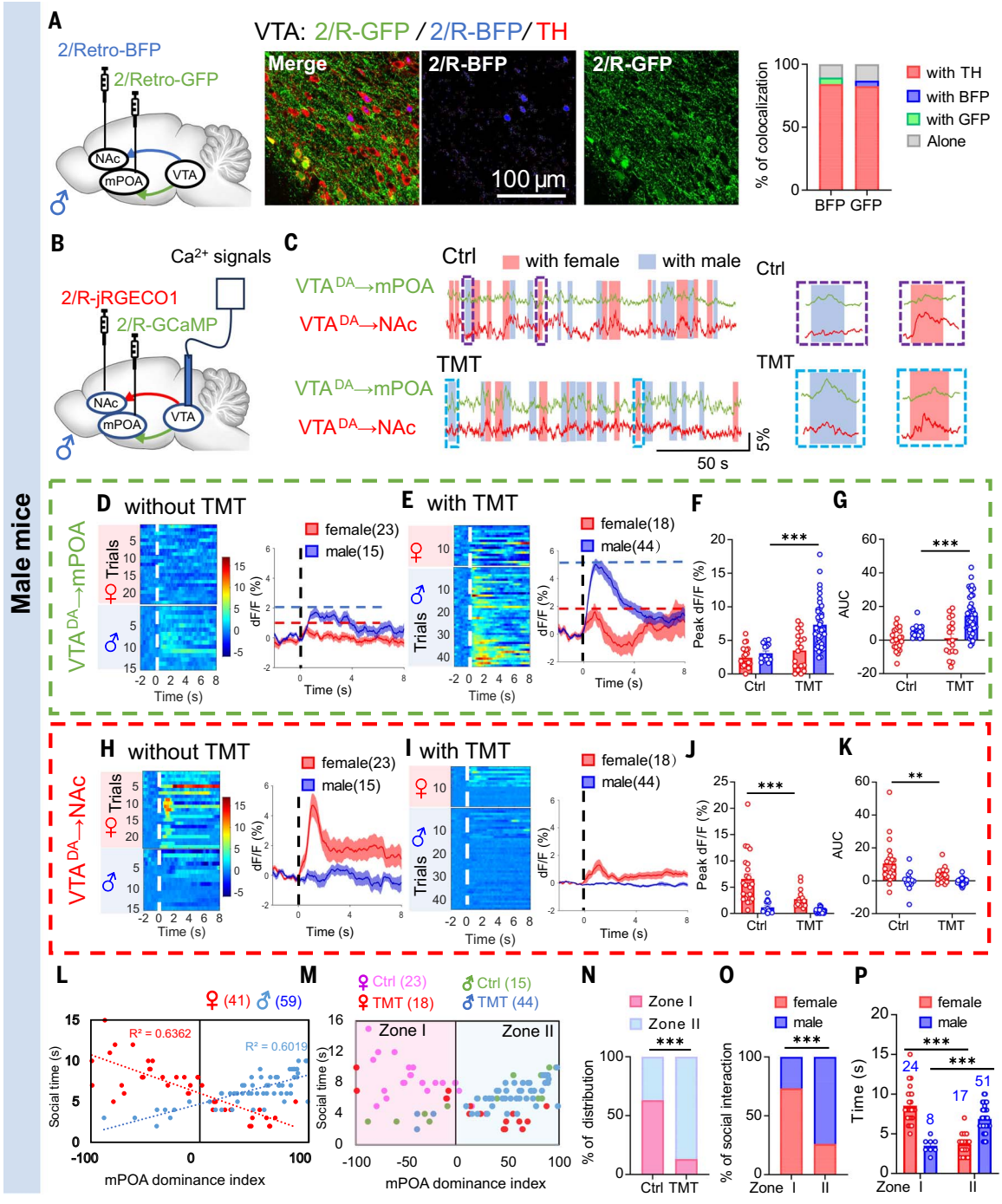

Fig. 5. The balance between VTA^{DA}-mPOA and VTA^{DA}-NAc projections determines sexual preference of males. (**A**) Schematic of retrograde virus injection in the NAc (carrying BFP) and the mPOA (carrying GFP) separately (left), representative micrographs (middle), and statistics showing distinct subpopulations of VTA^{DA} neurons projecting to the NAc and the mPOA in male mice (right). Scale bar, 100 μm. (**B** and **C**) Schematic of retrograde virus injection in the NAc (carrying jRGECO1) and the mPOA (carrying GCaMP), and representative traces of Ca^{2+} signals ($\Delta F/F_0$) of NAc-projecting (red) and mPOA-projecting (green) VTA^{DA} neurons in social-interacting male mice in the absence (Ctrl) or presence of TMT. The enlarged insets of the social interaction–coupled Ca^{2+} signals are shown on the right. (**D** to **G**) Heatmaps, averaged traces, and statistics of peak and AUC values of social interaction–coupled Ca^{2+} signals of mPOA-projecting VTA^{DA} neurons in male mice. (**H** to **K**) As shown in (D) to (G), except that Ca^{2+} signals of NAc-projecting VTA^{DA} neurons were recorded. (**L**) Pearson correlation analysis between social time (single interacting events) and the mPOA dominance index [calculated with the formula of Ca^{2+} signals as below: (VTA^{DA}→mPOA − VTA^{DA}→NAc)/(VTA^{DA}→mPOA + VTA^{DA}→NAc) × 100%] in male mice. (**M**) The distribution zones, as shown in (L), were divided into zone I and zone II by the equilibrium line of the mPOA dominance index. (**N** to **P**) Statistics of social events (Ctrl versus TMT; female- versus male-interaction events; female- versus male-interaction time) located in zone I and zone II. Data are presented as mean ± SEM. Two-way ANOVA for (F) to (K), and (P); Fisher's exact test for (A), (N), and (O). *P < 0.05, **P < 0.01, ***P < 0.001.

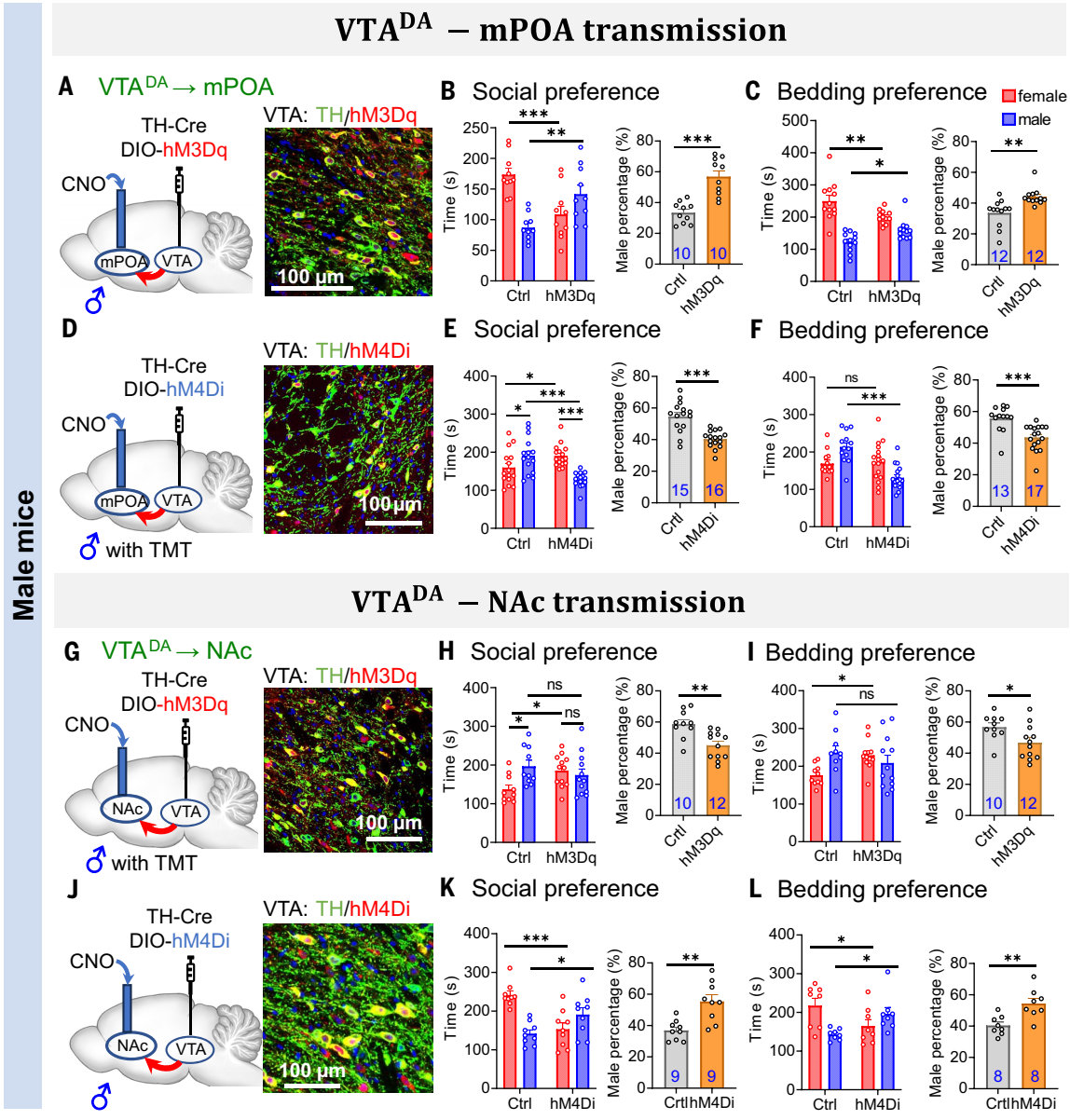

Fig. 6. VTA^{DA}-NAc and VTA^{DA}-mPOA pathways modulate sex preference in opposite directions in male mice. (**A** to **C**) Schematic of virus injection and cannula implantation, representative micrograph showing the colocalization of mCherry and TH-staining in the VTA, and statistics of social preference and bedding preference tests after the chemogenetic activation of VTA^{DA}-mPOA projection in male mice. Scale bar, 100 μm. (**D** to **F**) As shown in (A) to (C), except that chemogenetic inhibition of the VTA^{DA}-mPOA projection was used in male mice in the presence of TMT. (**G** to **L**) As shown in (A) to (F), except that chemogenetic manipulation was conducted on the VTA^{DA}-NAc projection in male mice. Data are presented as mean ± SEM. Two-way ANOVA for social time and unpaired Student's *t* test for male percentage. *P < 0.05, **P < 0.01, ***P < 0.001.

upon TMT exposure (Fig. 7J). These findings suggest that the higher excitability of the VTA^{DA}-NAc projection is underlying the preference switch of female mice, transitioning from same-sex interaction in control states to opposite-sex interaction when confronted with survival threats.

Firing patterns of VTA^{DA}-NAc projection determine the sociosexual preference of females

Why is the hyperactivity of VTA^{DA}-NAc projection positively correlated with both female (in the control state) and male (under survival threats) interactions? Because VTA^{DA} neurons exhibit two primary modes of firing activities, including the sustained low-frequency (typically ~5-Hz) tonic firing and the high-frequency (>10-Hz, usually <50-Hz) phasic firing with three to five spikes per burst (*55*–*57*), we speculated that the alteration between phasic versus tonic firing patterns may be responsible for the switching of social preference of female individuals. To test this hypothesis, a TH-driven GCaMP-expressing adeno-associated virus (AAV) vector was injected into the VTA and an optical fiber was implanted in the NAc for the specific recording of Ca^{2+} signals of VTA^{DA} projections in this area (Fig. 8A and fig. S11, A and B). Although both female and male interactions were correlated with Ca^{2+} transients of VTA^{DA} terminals in the NAc, female interaction–coupled Ca^{2+} transients were much stronger and had faster kinetics, indicative of the transient high-frequency or phasic-like action potential (AP) firings of VTA^{DA} neurons. However, the amplitude and AUC values of these Ca^{2+} transients were substantially reduced in the presence of TMT (Fig. 8, B and C). By contrast, male interactions were linked to Ca^{2+} signals with much slower kinetics, reflective of the sustained low-frequency or tonic-like AP firings of VTA^{DA} neurons. These signals were increased upon exposure to TMT (Fig. 8, B and C). Consistent with these observations, male interaction–coupled Ca^{2+} transients displayed a smaller rise rate and a larger half-height duration compared with those occurring during female interactions, irrespective of the presence or absence of TMT (Fig. 8D). These findings collectively suggest that the firing-pattern alteration of VTA^{DA} terminals in the NAc aligns with the sociosexual preference of female mice. On the basis of these results, we propose that phasic firing promotes female preference, whereas the survival threat of TMT exposure shifts the behavior to male preference

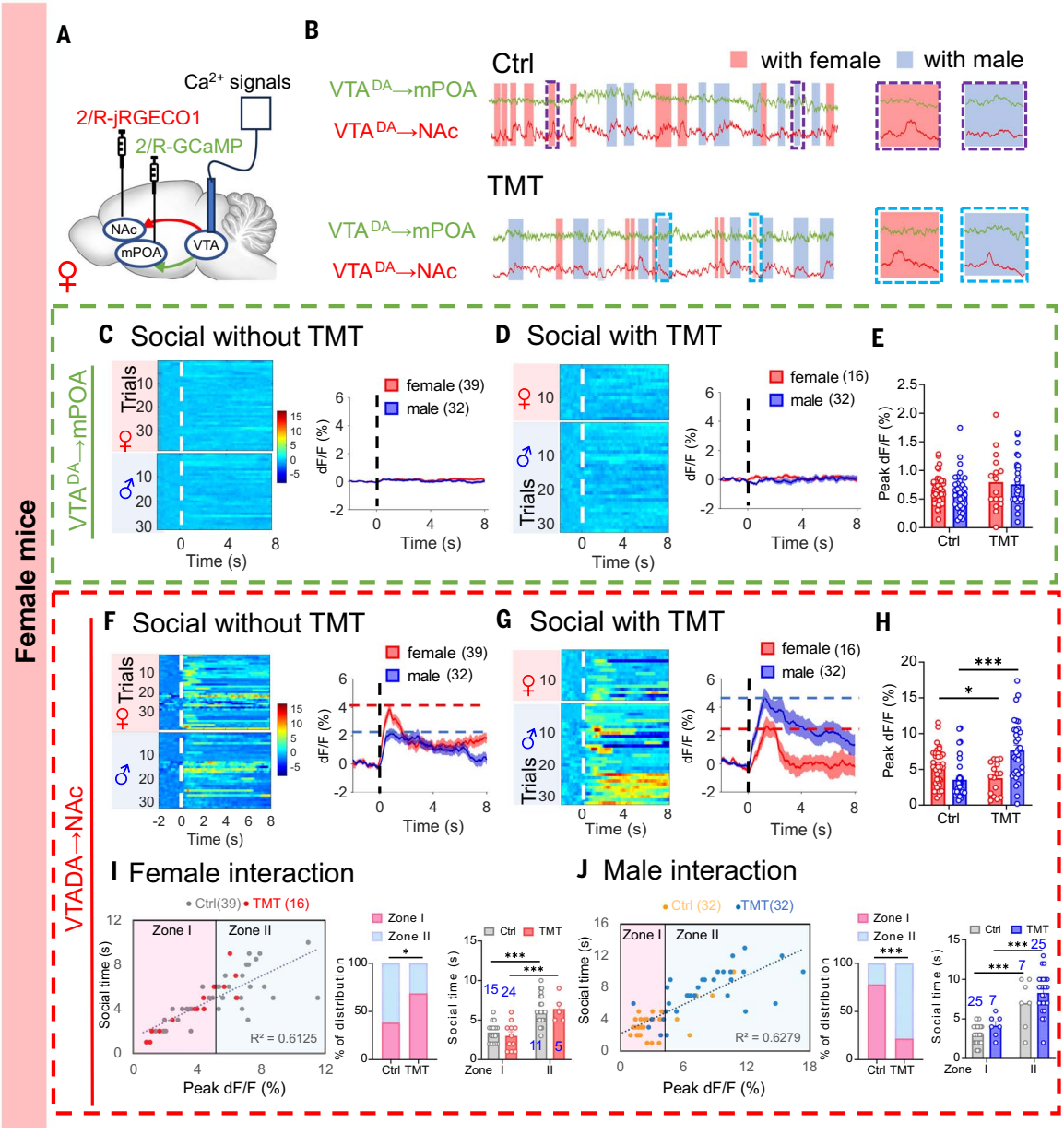

Fig. 7. Positive association of VTA^{DA}-NAc projection with both male and female interactions of female mice. (**A** and **B**) Schematic of retrograde virus injection in the NAc (carrying jRGECO1) and the mPOA (carrying GCaMP), and representative traces of Ca^{2+} signals ($\Delta F/F_0$) of NAc-projecting (red) and mPOA-projecting (green) VTA^{DA} neurons in social-interacting female mice in the absence (Ctrl) or presence of TMT (B). (**C** to **E**) Heatmaps, averaged traces, and statistics of social interaction–coupled Ca^{2+} signals of mPOA-projecting VTA^{DA} neurons in female mice. (**F** to **H**) As shown in (C) to (E), except that social interaction–coupled Ca^{2+} signals of NAc-projecting VTA^{DA} neurons were recorded. (**I**) Pearson correlation analysis between social time of female interacting events and the Ca^{2+} signals of NAc-projecting VTA^{DA} neurons, zone division by the 50% percentile of Ca^{2+} signals, and statistics of social events (social events and interacting time of single event in Ctrl versus TMT) located in zone I and zone II. (**J**) As shown in (I), except that male interacting events were used for analysis. Data are presented as mean ± SEM. Two-way ANOVA for (E) and (H) and social time analysis in (I) and (J); Fisher's exact test for social events distribution in (I) and (J). *P < 0.05, **P < 0.01, ***P < 0.001.

through the inhibition of phasic firing and the facilitation of tonic firing of these NAc-projecting VTA^{DA} neurons.

To test whether the firing pattern of VTA^{DA} neurons is a decisive factor in dictating the sex preference of female individuals, TH-Cre and Cre-dependent ChR2-expressing viral vectors were coinjected into the VTA, and a pair of optical fibers were implanted in the NAc to selectively elicit DA terminals with either phasic (20-Hz, five pulses, 1-s burst interval) or tonic (5-Hz) light stimulation (Fig. 8E and fig. S11, C and D). We found that, in control conditions, phasic stimulation of DA terminals in the NAc resulted in an increase in social time of female mice spent with females and a decrease in time spent with male animals, leading to a more pronounced female preference (Fig. 8F and fig. S11E). Similarly, phasic activation of VTA^{DA}-NAc projections in female mice also facilitated the preference for female bedding (fig. S11F). Conversely, mice that received tonic stimulation spent more time with males and less time with females, exhibiting increased male preference in the social preference test (Fig. 8G and fig. S11G). A similar phenomenon was observed in the bedding preference test (fig. S11H). These results confirmed that the firing-pattern alteration of NAc-projecting VTA^{DA} neurons determines the sex preference of female mice during social interaction, during which phasic firing promotes female preference and tonic firing facilitates male preference.

Although tonic versus phasic firing patterns of VTA^{DA} neurons have been reported to be functionally involved in motivation behavior and reward prediction (*58*–*61*), how the firing-pattern alteration determines social decision-making remains to be fully elucidated. To determine whether the altered DA release is underlying sex preference governed by different firing patterns, we performed electrochemical carbon-fiber electrode (CFE)–based amperometric recordings (*62*–*64*) in response to phasic or tonic optogenetic stimuli and found that repetitive phasic stimulation induced the release of larger DA transients, characterized by

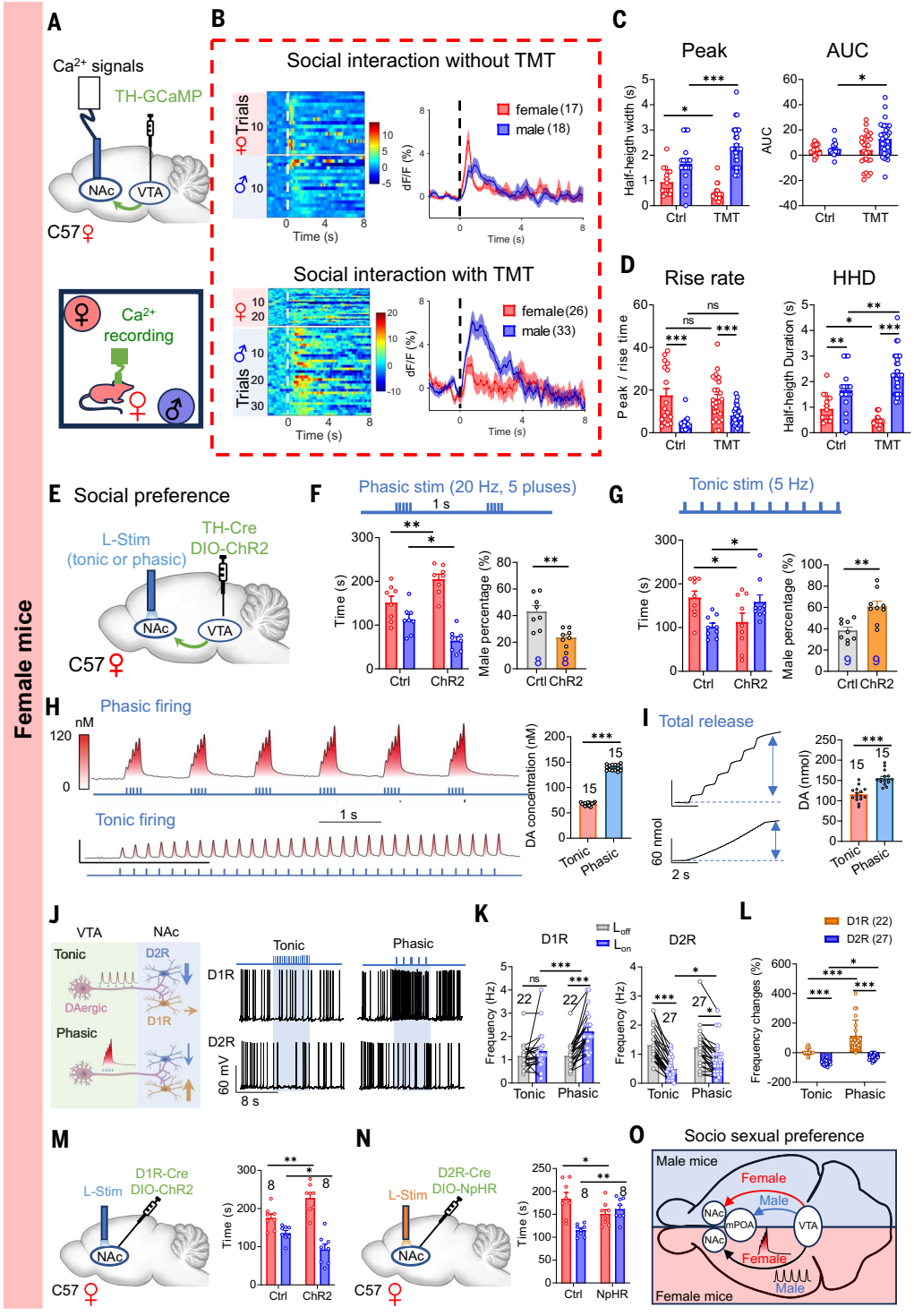

Fig. 8. The firing pattern alteration of VTA^{DA}-NAc projection determines sex preference of females. (**A**) Schematics of virus (TH-GCaMP) injection in the VTA and Ca^{2+} recordings in the NAc of the social-interacting female mice. (**B** to **D**) Heatmaps, averaged traces, and statistics of social interaction–coupled Ca^{2+} signals, including the peak, AUC, rise time, and half-height duration (HHD) of VTA^{DA} terminals in the NAc of female mice. (**E**) Schematics of virus (TH-Cre and DIO-ChR2) injection in the VTA and optical stimuli [light stimulation (L-stim), phasic or tonic] in the NAc. (**F** and **G**) Statistics of social preference test of female mice after phasic or tonic activation of VTA^{DA} terminals in the NAc. (**H**) CFE amperometry recordings of DA release with the calibrated heatmaps of DA concentration, and statistics of peak values of DA release in response to phasic or tonic L-stim. (**I**) Cumulative traces, and statistics of total DA release in the NAc in response to phasic or tonic L-stim as shown in (H). (**J**) Schematic showing the proposed DA transmission in response to phasic or tonic AP firing of DA terminals, and representative AP traces of D1R and D2R MSNs in the NAc. (**K** and **L**) Statistics of AP frequency and frequency changes of D1R and D2R MSNs in response to phasic or tonic L-stim. (**M**) Schematic of virus injection (D1R-Cre and DIO-ChR2) and optical fiber implantation in the NAc, and statistics of social interaction time of female mice after the L-stim (470 nm, 5 mW, 5-ms pulse at 20 Hz). (**N**) As shown in (M), except that optogenetic inhibition of D2R MSNs was used and the 580-nm L-stim (10 mW, continuous) was applied. (**O**) Working model showing the sexual dimorphic DA circuits involved in sociosexual preference. The balance between VTA^{DA}-NAc (female preference) and VTA^{DA}-mPOA (male preference, dominates when confronted with survival threats) projections determines the social decisions of male individuals, whereas the firing-pattern alteration of VTA^{DA} terminals and thus the biased DA transmission (phasic firing–facilitated D1R transmission mediates female preference, and tonic firing–dominated D2R transmission mediates male preference) in the NAc is utilized by females to determine their sociosexual preference. Data are presented as mean ± SEM. Two-way ANOVA for (C) to (G) and (K) to (N), unpaired Student's *t* test for (H) and (I) and male percentage in (F) and (G), and paired Student's *t* test for L-stim effects in (K). *P < 0.05, **P < 0.01, ***P < 0.001.

robust periodic fluctuations (Fig. 8H and fig. S11I). By contrast, the same number of AP-like tonic stimuli induced a lower sustained release of DA (Fig. 8H and fig. S11J), reflecting the steady and continuous DA release associated with tonic firing. Consistent with this, phasic stimulus led to a much higher local DA concentration and thus more total DA release compared with that resulting from the tonic stimulus (Fig. 8, H and I). Thus, the firing pattern alteration of VTA^{DA} neurons determines the sex preference of female mice most probably through the modulation of local DA fluctuations.

Considering that DA transmission in the NAc is mediated via either the inhibitory D2R

(type 2 DA receptor) or the excitatory D1R (type 1 DA receptor) and that the D2R has a ~10-fold-higher binding affinity to DA than does the D1R (*65*, *66*), we propose that different DA fluctuations might determine social decisions through their distinct modulation of downstream D1R and D2R medium spiny neurons (MSNs) in the NAc. To test this idea, we conducted whole-cell patch clamp AP recordings of D1R and D2R MSNs in response to the optogenetic activation of VTA^{DA} terminals in the NAc (Fig. 8J). We found that a phasic stimulus, but not a tonic stimulus, led to the robust increase in AP frequency of D1R MSNs (Fig. 8, J and K). Conversely, tonic stimuli resulted in a much more pronounced inhibition of D2R MSNs compared with phasic stimuli (Fig. 8, J and K). Thus, D1R MSNs are specifically responsive to the transient, large DA fluctuations associated with phasic firing of DA terminals, whereas D2R MSNs are more sensitive to the sustained DA release resulting from prolonged tonic firing of DA terminals (Fig. 8L).

To further confirm that the two types of MSNs are sufficient to mediate the sociosexual preference of female mice, we used an optogenetic strategy (coinjection of D1R/D2R-Cre and Cre-dependent ChR2-expressing viral vectors) to selectively manipulate D1R and D2R MSNs in the NAc (Fig. 8, M and N, and fig. S12, A and D). Optogenetic excitation of D1R MSNs, which mimics the phasic firing of DA terminals, further increased social time with females, resulting in decreased preference for males by female animals (Fig. 8M and fig. S12B). By contrast, optogenetic inhibition of D2R MSNs, which mimics the tonic firing of DA terminals, led to the switch of female animals' social preference from female to male (Fig. 8N and fig. S12E). Similar results were obtained in the bedding preference test (fig. S12, C and F). Additionally, similar results were achieved when D2R-Cre viral vectors were replaced with a virus carrying A2A-Cre (fig. S12, G to I). Collectively, these findings suggest that females make the social decision through the balance between phasic firing–facilitated DA-D1R transmission and tonic firing–dominated DA-D2R transmission in the NAc.

Discussion

Social interaction between different sexes is a fundamental aspect of life for most species because it plays an essential role in reproduction, survival, and evolution. In this study, we found that males prefer social interaction with females, which is probably driven by the innate needs of mating and reproduction. Females also show a preference for female encounters under control conditions. This has been observed in both rodents (*33*) and humans (such as bosom friends) (*67*, *68*), which might stem from the long-term evolution of the same-sex social collaborations in activities such as maternal support, emotional sustenance, and consolation. However, in the presence of survival stress or in a hostile or challenging environment, both sexes shift their preference toward male interactions, through which they may reach a maximal benefit from social protection. Thus, sociosexual preference is an adaptive response to the specific environment in which they live, and this preference can be convergently refined by the internal-drive condition and external-environment context to ensure survival and species continuation in rapidly changing environments.

Although critical roles of the mesolimbic DA system in reward, motivation, and social interaction have been well-established (*14*, *40*, *41*), its involvement in shaping sociosexual preference remains largely unknown. In the present work, we demonstrated a strong link between the excitability of VTA^{DA} neurons and the shift in sex preference under survival stress. Our findings define the mesolimbic DA system as a key pivotal hub for sex preference in social decision-making, which may explain how animals or humans can make appropriate social decisions to get the maximal benefits, especially when they encounter conflicts between innate requirements and external survival threats.

Male and female individuals utilize very different schemes for the neural coding of social preferences. The competition between different VTA^{DA}-projecting circuits was used by males to encode their sociosexual preference; the VTA^{DA}-NAc projection is predominant under control conditions to promote female preference, whereas the activities of VTA^{DA}-mPOA projection can be enhanced by survival threats to facilitate social interaction with male individuals (Fig. 8O). These findings support the notion that the VTA^{DA}-NAc reward pathway may play crucial roles in the innate requirements of males for mating and reproduction, whereas the defensive VTA^{DA}-mPOA pathway can be activated by survival threats and thus leads to male preference, which may contribute to forming a stronger protective network for individual survival and population continuity. By contrast, the firing-pattern alteration of the VTA^{DA}-NAc projection is utilized by females to determine their sex preference. Phasic firing–like excitation of VTA^{DA} neurons promotes female preference through the facilitated D1R transmission in the NAc; however, environmental threats lead to male preference through the enhanced tonic firing–like excitation of DA neurons and thus the predominant DA-D2R transmission in the NAc (Fig. 8O). Thus, these findings not only elucidate the sex-binary properties of VTA^{DA} neurons in terms of neural circuit integration and firing-pattern alteration but also highlight critical roles of this sexually dimorphic DA system in mediating social preference shifts in response to survival threats; they also provide valuable insights into the neural mechanisms that govern social decision-making and its modulation by environmental factors.

How could the dimorphic DA circuits contribute to the determination of social preference? Although male and female individuals utilize different strategies to encode their social decisions on sex selectivity, their preference can be similarly modulated by different survival stressors even when those stressors are transduced via distinct sensory pathways such as olfaction (TMT), vision (contextual FC), and auditory (cued FC). How these sensory inputs converge onto specific subpopulations of VTA^{DA} neurons and how their firing patterns can be modified by external survival stresses deserve systematic investigations in the future. It would also be intriguing to explore whether the VTA^{DA}-NAc and VTA^{DA}-mPOA projections are selectively activated in other species such as nonhuman primates and humans and how this selectivity may contribute to their sociosexual preferences. Further studies are needed to examine the extent to which these projections are involved in other aspects of social decisions, such as social avoidance, social preference, social support, and social hierarchy. It would also be interesting to test whether and how sex preference can be modulated by other physiological conditions or by external conditions such as extreme climate changes, food deprivation, and social stress exposure (*69*).

Taken together, our study reveals that both sexes exhibit female preference during social interaction but switch to male preference under survival threats, indicating an adaptive shift in social decision-making. However, they utilize very different schemes for the neural coding of social preference. This study not only establishes critical roles of DA transmission in social decision-making and defines the sexually dimorphic DA circuit mechanisms underlying sex preference but also provides a conceptual framework for understanding how social decisions can be convergently determined by the balance between innate requirements and external survival threats.

Materials and methods

Animals

Adult (~3 months) male and female (non-estrus) C57/BL6 mice were from Charles River (Beijing). DAT-Cre transgenic mice were from Jackson lab (JAX: 006660). Female mice used in this work were all non-estrous virgin females. The animals were housed in the animal facility with a maximum of five mice per cage under a 12-hour light-dark cycle at a consistent temperature of 22° ± 2°C and were provided with food and water ad libitum. The use and care of animals were approved and directed by

the Animal Care and Use Committee of Xi'an Jiaotong University.

Stereotaxic surgery

Stereotaxic surgery was performed as previously described (*14*, *62*, *63*). The mice were anesthetized with avertin (1.5% tribromoethanol, 2.5% tertiary butanol, and 0.9% NaCl; 0.1 ml/5 g body weight). Mice were fixed in a stereotaxic frame (RWD Instruments, China) for precise surgical manipulation. The skull was exposed by making a midline incision, and cleaned with hydrogen peroxide to expose the bregma and lambda for head position adjustment. A cranial drill (RWD Instruments, China) was used to create small cranial windows for the implantation of guide cannulas (RWD Instruments, China), optical fibers (Inper, China), or for virus injection. For virus injection, the virus (each 200 to 300 nl) was injected into the target area at 100 nl min^{-1} through a glass pipette. The pipettes were left in place for 10 min post-injection. After surgery, the skin was sutured, and animals were placed on a heating plate (KEL-2000, Nanjing, China) at 37°C for recovery. Three weeks later, when required, mice were anesthetized and fixed on a stereotaxic frame for the implantation of the guide cannulas or optical fibers using similar stereotaxic procedures.

Slice preparation

The general methods for preparing NAc slices were similar to those described previously (*62*, *70*). Mice were anaesthetized with tribromoethanol via intraperitoneal injection (0.2 ml/10 g). Then, the whole brain was quickly removed into ice-cold cutting solution (in mM): 110 $C_5H_{14}ClNO$, 2.5 KCl, 0.5 $CaCl_2$, 7.0 $MgCl_2$, 1.3 NaH_2PO_4, 25 $NaHCO_3$, 10 D-(+)-glucose, saturated with 95% O_2 and 5% CO_2. Additional 1.3 L-ascorbate ($C_6H_8O_6$), 0.6 Na-pyruvate ($C_3H_3NaO_3$) were included for whole-cell patch clamp recordings. Then, horizontal slices containing the NAc were cut at 300 μm using a vibratome (Leica VT 1200s). The slices were transferred into artificial cerebrospinal fluid (aCSF, in mM): 125 NaCl, 2.5 KCl, 2.0 $CaCl_2$, 1.3 $MgCl_2$, 1.3 NaH_2PO_4, 25 $NaHCO_3$, 10 D-(+)-glucose, saturated with 95% O_2/5% CO_2 (additional 1.3 $C_6H_8O_6$, 0.6 $C_3H_3NaO_3$ for whole-cell patch clamp recording) and incubated at 37°C for 30 min, followed by an additional 30 min at room temperature before recording.

Whole-cell patch clamp recording

Whole-cell patch clamp recordings were performed as described previously (*62*, *63*). Neurons in brain slices were visualized under an upright microscope (BX51W1, Olympus) using a 60× water-immersion lens, along with an infrared-differential interference contrast and an infrared camera (IR-2000) connected to the video monitor. Slices were perfused with aCSF at a rate of 1.5 ml/min. Somatic patch-clamp signals (action potentials, APs) were recorded under whole-cell configuration using an EPC10/2 amplifier under the control of PatchMaster version 2X90.2 software (HEKA Electronik, Germany). Signals were digitized at 20 kHz and low-pass filtered at 2.9 kHz. The pipettes were pulled with a PC-10 glass micropipette puller (Narishige, Japan) to achieve resistances of 3 to 5 MΩ. The intracellular pipette solution contained (in mM) 120 K^+-Glucose, 5 NaCl, 10 HEPES, 1 $MgCl_2$, 0.2 EGTA, 2 MgATP, 0.1 Na_3GFP, 10 phosphocreatine, with pH adjusted to 7.2, and 305 mOsm. Optical stimulation (589 nm, continuous; or 488 nm at 5 Hz) was delivered using laser generators (Beijing Viasho Technology, China) through an optical fiber (200 μm in diameter) positioned ~200 μm from the slice surface. Drugs were delivered with a multichannel perfusion system (World Precision Instruments, Sarasota). All recordings were made at room temperature. Data were analyzed with Igor Pro 6.22 software (Wavemetrics, Lake Oswego, OR), with series conductance and membrane conductance monitored to ensure the seal condition of patch-clamp recordings.

Amperometric DA recording in brain slices

Amperometric recordings in slices were made as described previously with small modifications (*62*–*64*). CFEs with a diameter of 7 μm which had an exposed sensor tip of ~200 μm were used to measure DA release. The exposed sensor tip was completely inserted into the tissue of NAc slices and a holding potential of 780 mV was applied using an EPC10/2 amplifier under the control of Pulse software PatchMaster v2x90.2 (HEKA Electronic, Germany). DA release in the NAc was evoked by using 470-nm yellow light with specific stimulation patterns to mimic phasic (20-Hz, five spikes/burst, 1-s burst-interval) or tonic (5-Hz, sustained spikes) AP firings. The amperometric current (I_{amp}) was low-pass filtered at 100 Hz and digitized at 3.13 kHz. Off-line data analysis was performed using Igor software (WaveMetrix).

Optogenetic and chemogenetic manipulation in vivo

To perform chemogenetic manipulation (*62*, *71*), pAAV-EF1α-DIO-hM3D(Gq)-EGFP-WPRE (AAV2/9, 1.0 × 10^{12} vg ml^{-1}) or pAAV-EF1α-DIO-hM4D (Gi)-EGFP-WPRE (AAV2/9, 1.0 × 10^{12} vg ml^{-1}) mixed with rAAV-TH-NLS-CRE-WPRE-hGH pA (AAV2/9, 1.0 × 10^{12} vg ml^{-1}) were injected into the VTA of male/female mice. After a recovery period of 3 weeks, guide cannulas (internal diameter of 1.25 mm) were implanted into the NAc or mPOA for the local application of CNO, and the mice were allowed to recover for 1 week prior to behavioral experiments. A stainless-steel injector attached to a 10-μl syringe and an infusion pump was inserted into the guide cannula. CNO (3 μM, 0.5 μl) was infused at a rate of 100 nl min^{-1} under the control of a micro-injection pump (R462, RWD Instruments, China). The injector was slowly withdrawn 2 min after the infusion, and behavioral tests were performed 5 min after the microinjection.

For the optogenetic manipulation (*45*, *63*, *72*), rAAV-EF1α-DIO-hChR2(H134R)-EYFP-WPRE-hGH pA (AAV2/9, 1.0 × 10^{12} vg ml^{-1}) mixed with rAAV-TH-NLS-CRE-WPRE-hGH pA (AAV2/9, 1.0 × 10^{12} vg ml^{-1}) were injected into the VTA of female mice. Three weeks later, an optical fiber was implanted in the NAc for the delivery of light stimuli. The mice were allowed to recover for 1 week prior to behavioral tests. The delivery of a train of stimuli with 470-nm blue light (20 Hz, five spikes/burst, 1-s burst-interval; or 5 Hz, sustained spikes) was controlled by a Master-8 pulse stimulator (Hangzhou Newton Technology, China).

Optical fiber photometry

The Ca^{2+} transient signal was measured using a custom-built fiber photometry system (QAXK-FPS-SS-LED-OG, ThinkerTech, China) as described previously (*62*, *73*). To record the somatic Ca^{2+} signal of VTA^{DA} neurons, rAAV-EF1α-DIO-GCaMp6s-WPRE-hGH pA (PT-0017, BrainVTA, China) mixed with rAAV-TH-NLS-CRE-WPRE-hGH pA (PT-0179, BrainVTA, China) were injected into the VTA and an optical fiber was implanted in the VTA. For simultaneous recording of the somatic Ca^{2+} signals of NAc- and mPOA-projecting VTA^{DA} neurons, rAAV-hSyn-GCaMp6s-WPRE-hGH polyA, 2/Retro (PT-0145, BrainVTA, China) was injected into the mPOA and rAAV-hSyn-jRGECO1a-WPRE (PT-6767, BrainVTA, Wuhan, China) was injected into the NAc. An optical fiber (Inper, Hangzhou, China) was implanted into the VTA to record the somatic Ca^{2+} signals in VTA^{DA} neurons 3 weeks after virus injection. To record the Ca^{2+} signal of VTA^{DA} terminals in the NAc, we injected rAAV-EF1α-DIO-GCaMp6s-WPRE-hGH pA mixed with rAAV-TH-NLS-CRE-WPRE-hGH pA into the VTA and implanted an optical fiber in the NAc. The mice were allowed 1 week recovery before Ca^{2+} signal recording.

During the recording test, a female stranger mouse was put in a mesh cage on the corner of an open field, and a male stranger mouse was placed on the diagonal opposite side. The test mouse was placed in the center of the open field and allowed to explore freely. Social interaction included both nose-to-nose interaction and body-sniffing (tail, body, and paw) of the caged mice by the testing mice. The time points that the experiment mice interacted with female/male caged mice were manually recorded. The 470-nm and 580-nm laser beams were reflected off a dichroic mirror and focused with an objective lens to excite the calcium indicators GCaMP6s and jRGECO1a, respectively. The Ca^{2+} signals were collected with a

photomultiplier tube and converted into electrical signals using customized acquisition software written in NI Lab View (National Instruments). The changes of Ca^{2+} signals were evaluated using $\Delta F/F$ values, where $\Delta F/F = \frac{(F-F_{mean})}{F_{mean}} \times 100\%$. F_{mean} was the average fluorescence intensity (baseline) before laser stimulation. Recording results were analyzed with custom MATLAB (MathWorks, Natick, MA, USA) MAT files produced by Thinker Biotech.

Immunochemistry

Immunohistochemistry was applied as described previously (*62*, *63*, *74*). Briefly, mice were anesthetized with avertin and perfused with ice-cold phosphate-buffered saline (PBS) containing 4% paraformaldehyde (PFA) for tissue fixation. The brain was removed and immersed in 4% PFA at 4°C for 24 hours. After dehydration in 10, 20, and 30% sucrose, a series of 30-μm coronal slices across the VTA/NAc/mPOA were cut using a Thermo cryostat (RWD instruments, China). The slices were rinsed three times with PBS and permeabilized with 0.3% Triton X-100 in PBS containing 2% BSA for 5 min at room temperature. After blocking with 10% FBS in PBS for 2 hours, the slices were incubated with primary antibodies at 4°C overnight. The following primary antibodies were used as indicated: anti-tyrosine hydroxylase (AB1542, Sigma-Aldrich), and anti-cFos (SYS-226-308, SYSY). The slices were washed three times with blocking solution and then incubated with secondary antibodies (Rabbit Anti-Guinea Pig IgG (HL) - Alexa Fluor 594, M213619S, Abmart; Alexa Fluor 488 donkey anti-rabbit IgG (H+L), A-21206; Alexa Fluor 647 goat anti-rabbit IgG (H+L), A-21070, Invitrogen) for 1 hour. Finally, slices were mounted on slides with DAPI/Antifade solution (S7113, Sigma) and fluorescence images were captured using a Leica TCS SP8 STED microscope (Leica, Germany). Images were analyzed with ImageJ (National Institutes of Health, Bethesda, MD).

Behavioral tests

The procedures for behavioral tests were as described previously (*62*, *74*). All behavioral tests were conducted at the early stage of dark phase (20:00 to 22:00). The animals were transported into the testing room in a holding cage to acclimate for at least 1 hour before testing. Their behaviors were monitored using a video tracking system (SMART, Panlab, USA) and later analyzed with video analysis software. The testing room was kept at a low light (~20 lux) to minimize anxiety. To avoid the adaptation effects and experience-dependent responses, we used different populations of mice for different behavioral assays.

Social/bedding preference test

The social preference test was performed in a Plexiglas rectangular box (60 cm by 40 cm by 22 cm) with three interconnected chambers of equal size as described previously (*75*). The test mouse was placed in the center chamber and allowed to explore the box for 10 min with both gates to the side chambers closed. This design helped in minimizing the influence of prior exposure to the test room, and it also helped in establishing a consistent environment for all the behavioral tests. A female stranger mouse was introduced in a mesh cage in one side chamber, and a male stranger mouse was placed in a similar mesh cage in the other side chamber. When applicable, TMT was placed at the central region 30 cm above the apparatus to serve as a survival stressor. The test mouse was then allowed to freely explore the three interconnected chambers for a total of 10 min. The time the test mouse spent interacting with each sex (5 cm nearby the mesh cages) was automatically recorded by using the SMART software (Panlab, USA). The social preference index (male percentage) was calculated by dividing the sniffing time with the male stranger by the total sniffing time with both mice, as previously described (*76*).

Similar to social preference, in the bedding preference test, the bedding from female or male strangers was used instead of the caged mice in each side of the chamber. The test mouse was then allowed to freely explore the three interconnected chambers for 10 min. The time the test mouse spent sniffing and approaching the male or female bedding materials was recorded. The bedding preference index (male percentage) was calculated by dividing the sniffing time with the male bedding by the total sniffing time with the bedding on both sides.

Cued and contextual fear conditoning test

The cued and contextual test was performed as described previously (*77*). The pre-conditioning was conducted in an experiment chamber (30 cm by 30 cm by 40 cm) with an electrified grid floor. The testing mouse was placed in the chamber and allowed to explore freely for 1 min. Then the mouse was exposed to a neutral stimulus (tone, for 2 s), which is followed by a paired aversive stimulus (electric shock, 0.3 mA for 1 s, twice in 2 min). The experimental chamber used in training procedure was used for the contextual FC test to ensure exactly the same context. A female stranger mouse was put in a mesh cage in one corner and a male stranger mouse was caged on the diagonal opposite side. The fear-conditioned mouse was then put into the experimental chamber and allowed to explore freely for 10 min. The cued FC test was performed in a three-chamber box, in which female and male stranger mice were placed in the side cages, and the fear-conditioned mouse was placed in the middle cage and allowed to explore the three chambers in free for 10 min. During the exploration period, the tone was periodically introduced once per minute. The time the testing mice spent interacting with each sex (5 cm nearby the mesh cages) was automatically recorded by using the SMART software (Panlab, USA), and the social preference index (male percentage) was calculated by dividing the sniffing time with the male stranger by the total sniffing time with both mice.

Statistics

All experiments were performed meticulously with at least three biological repeats and conducted in a randomized order to avoid confounding factors. The behavioral tests were applied and analyzed in a double-blind manner. Appropriate sample sizes were chosen based on data variability and the literature. No samples or animals that provided successful measurements were excluded from analysis. The data were presented as the mean ± SEM, and statistical comparisons were made using the two-tailed unpaired Student's *t* test, Kolmogorov-Smirnov test, two-way ANOVA (followed by Sidak's multiple comparisons), or Pearson correlation analysis as indicated. Data normality was assessed by using the Shapiro-Wilk test, and the variance equality was determined with Levene's test. All statistical analyses were performed using GraphPad Prism 8.0, and significant differences were accepted at $P < 0.05$. Numbers of mice, slices, or cells analyzed are indicated in the figures.

REFERENCES AND NOTES

1. J. J. Walsh, D. J. Christoffel, R. C. Malenka, Neural circuits regulating prosocial behaviors. *Neuropsychopharmacology* **48**, 79–89 (2023). doi: 10.1038/s41386-022-01348-8; pmid: 35701550
2. Z. Guo *et al*., Neural dynamics in the limbic system during male social behaviors. *Neuron* **111**, 3288–3306.e4 (2023). doi: 10.1016/j.neuron.2023.07.011; pmid: 37586365
3. J. T. Kwon *et al*., An amygdala circuit that suppresses social engagement. *Nature* **593**, 114–118 (2021). doi: 10.1038/s41586-021-03413-6; pmid: 33790466
4. L. Kingsbury *et al*., Correlated Neural Activity and Encoding of Behavior across Brains of Socially Interacting Animals. *Cell* **178**, 429–446.e16 (2019). doi: 10.1016/j.cell.2019.05.022; pmid: 31230711
5. T. H. Miller *et al*., Social Status-Dependent Shift in Neural Circuit Activation Affects Decision Making. *J. Neurosci.* **37**, 2137–2148 (2017). doi: 10.1523/JNEUROSCI.1548-16.2017; pmid: 28093472
6. L. A. O'Connell, H. A. Hofmann, Evolution of a vertebrate social decision-making network. *Science* **336**, 1154–1157 (2012). doi: 10.1126/science.1218889; pmid: 22654056
7. M. Liu, D. W. Kim, H. Zeng, D. J. Anderson, Make war not love: The neural substrate underlying a state-dependent switch in female social behavior. *Neuron* **110**, 841–856.e6 (2022). doi: 10.1016/j.neuron.2021.12.002; pmid: 34982958
8. C. Zhang *et al*., Dynamics of a disinhibitory prefrontal microcircuit in controlling social competition. *Neuron* **110**, 516–531.e6 (2022). doi: 10.1016/j.neuron.2021.10.034; pmid: 34793692
9. D. Lee, H. Seo, Neural Basis of Strategic Decision Making. *Trends Neurosci.* **39**, 40–48 (2016). doi: 10.1016/j.tins.2015.11.002; pmid: 26688301
10. J. LeDoux, N. D. Daw, Surviving threats: Neural circuit and computational implications of a new taxonomy of defensive behaviour. *Nat. Rev. Neurosci.* **19**, 269–282 (2018). doi: 10.1038/nrn.2018.22; pmid: 29593300
11. G. K. Adams, K. K. Watson, J. Pearson, M. L. Platt, Neuroethology of decision-making. *Curr. Opin. Neurobiol.* **22**, 982–989 (2012). doi: 10.1016/j.conb.2012.07.009; pmid: 22902613

12. I. Carta, C. H. Chen, A. L. Schott, S. Dorizan, K. Khodakhah, Cerebellar modulation of the reward circuitry and social behavior. *Science* **363**, eaav0581 (2019). doi: 10.1126/science.aav0581; pmid: 30655412
13. L. A. Gunaydin *et al*., Natural neural projection dynamics underlying social behavior. *Cell* **157**, 1535–1551 (2014). doi: 10.1016/j.cell.2014.05.017; pmid: 24949967
14. C. Solié, B. Girard, B. Righetti, M. Tapparel, C. Bellone, VTA dopamine neuron activity encodes social interaction and promotes reinforcement learning through social prediction error. *Nat. Neurosci.* **25**, 86–97 (2022). doi: 10.1038/s41593-021-00972-9; pmid: 34857949
15. V. Rappeneau, F. Castillo Díaz, Convergence of oxytocin and dopamine signalling in neuronal circuits: Insights into the neurobiology of social interactions across species. *Neurosci. Biobehav. Rev.* **161**, 105675 (2024). doi: 10.1016/j.neubiorev.2024.105675; pmid: 38608828
16. W. C. Huang, A. Zucca, J. Levy, D. T. Page, Social Behavior Is Modulated by Valence-Encoding mPFC-Amygdala Sub-circuitry. *Cell Rep.* **32**, 107899 (2020). doi: 10.1016/j.celrep.2020.107899; pmid: 32668253
17. P. Gangopadhyay, M. Chawla, O. Dal Monte, S. W. C. Chang, Prefrontal-amygdala circuits in social decision-making. *Nat. Neurosci.* **24**, 5–18 (2021). doi: 10.1038/s41593-020-00738-9; pmid: 33169032
18. J. K. Rilling, A. G. Sanfey, The neuroscience of social decision-making. *Annu. Rev. Psychol.* **62**, 23–48 (2011). doi: 10.1146/annurev.psych.121208.131647; pmid: 20822437
19. R. K. Hu *et al*., An amygdala-to-hypothalamus circuit for social reward. *Nat. Neurosci.* **24**, 831–842 (2021). doi: 10.1038/s41593-021-00828-2; pmid: 33820999
20. O. Dal Monte, C. C. J. Chu, N. A. Fagan, S. W. C. Chang, Specialized medial prefrontal-amygdala coordination in other-regarding decision preference. *Nat. Neurosci.* **23**, 565–574 (2020). doi: 10.1038/s41593-020-0593-y; pmid: 32094970
21. B. Dai *et al*., Responses and functions of dopamine in nucleus accumbens core during social behaviors. *Cell Rep.* **40**, 111246 (2022). doi: 10.1016/j.celrep.2022.111246; pmid: 36001967
22. H. Seo, D. Lee, Neural basis of learning and preference during social decision-making. *Curr. Opin. Neurobiol.* **22**, 990–995 (2012). doi: 10.1016/j.conb.2012.05.010; pmid: 22704796
23. S. Jang *et al*., Impact of the circadian nuclear receptor REV-ERBα in dorsal raphe 5-HT neurons on social interaction behavior, especially social preference. *Exp. Mol. Med.* **55**, 1806–1819 (2023). doi: 10.1038/s12276-023-01052-7; pmid: 37537215
24. M. M. Rogers-Carter *et al*., Insular cortex mediates approach and avoidance responses to social affective stimuli. *Nat. Neurosci.* **21**, 404–414 (2018). doi: 10.1038/s41593-018-0071-y; pmid: 29379116
25. A. Nair *et al*., An approximate line attractor in the hypothalamus encodes an aggressive state. *Cell* **186**, 178–193.e15 (2023). doi: 10.1016/j.cell.2022.11.027; pmid: 36608653
26. T. Karigo *et al*., Distinct hypothalamic control of same- and opposite-sex mounting behaviour in mice. *Nature* **589**, 258–263 (2021). doi: 10.1038/s41586-020-2995-0; pmid: 33268894
27. X. Jiang, Y. Pan, Neural Control of Action Selection Among Innate Behaviors. *Neurosci. Bull.* **38**, 1541–1558 (2022). doi: 10.1007/s12264-022-00886-x; pmid: 35633465
28. S. Fang *et al*., Sexually dimorphic control of affective state processing and empathic behaviors. *Neuron* **112**, 1498–1517.e8 (2024). doi: 10.1016/j.neuron.2024.02.001; pmid: 38430912
29. P. Chen, W. Hong, Neural Circuit Mechanisms of Social Behavior. *Neuron* **98**, 16–30 (2018). doi: 10.1016/j.neuron.2018.02.026; pmid: 29621486
30. S. W. Newman, The medial extended amygdala in male reproductive behavior. A node in the mammalian social behavior network. *Ann. N. Y. Acad. Sci.* **877**, 242–257 (1999). doi: 10.1111/j.1749-6632.1999.tb09271.x; pmid: 10415653
31. L. Kamas, A. Preston, Can social preferences explain gender differences in economic behavior? *J. Econ. Behav. Organ.* **116**, 525–539 (2015). doi: 10.1016/j.jebo.2015.05.017
32. E. H. M. Sterck, D. P. Watts, C. P. van Schaik, The Evolution of Female Social Relationships in Nonhuman Primates. *Behav. Ecol. Sociobiol.* **41**, 291–309 (1997). doi: 10.1007/s002650050390
33. Y. Liu *et al*., Molecular regulation of sexual preference revealed by genetic studies of 5-HT in the brains of male mice. *Nature* **472**, 95–99 (2011). doi: 10.1038/nature09822; pmid: 21441904
34. J. Wang *et al*., Basal forebrain mediates prosocial behavior via disinhibition of midbrain dopamine neurons. *Proc. Natl. Acad. Sci. U.S.A.* **118**, e2019295118 (2021). doi: 10.1073/pnas.2019295118; pmid: 33563763
35. Y. Beny-Shefer *et al*., Nucleus Accumbens Dopamine Signaling Regulates Sexual Preference for Females in Male Mice. *Cell Rep.* **21**, 3079–3088 (2017). doi: 10.1016/j.celrep.2017.11.062; pmid: 29241537
36. E. S. Bromberg-Martin, M. Matsumoto, O. Hikosaka, Dopamine in motivational control: Rewarding, aversive, and alerting. *Neuron* **68**, 815–834 (2010). doi: 10.1016/j.neuron.2010.11.022; pmid: 21144997
37. F. Sun *et al*., A Genetically Encoded Fluorescent Sensor Enables Rapid and Specific Detection of Dopamine in Flies, Fish, and Mice. *Cell* **174**, 481–496.e19 (2018). doi: 10.1016/j.cell.2018.06.042; pmid: 30007419
38. J. B. Becker, C. N. Rudick, W. J. Jenkins, The role of dopamine in the nucleus accumbens and striatum during sexual behavior in the female rat. *J. Neurosci.* **21**, 3236–3241 (2001). doi: 10.1523/JNEUROSCI.21-09-03236.2001; pmid: 11312308
39. W. J. Jenkins, J. B. Becker, Dynamic increases in dopamine during paced copulation in the female rat. *Eur. J. Neurosci.* **18**, 1997–2001 (2003). doi: 10.1046/j.1460-9568.2003.02923.x; pmid: 14622232
40. J. S. Flannery *et al*., Developmental Changes in Habenular and Striatal Social Reinforcement Responsivity Across Adolescence Linked With Substance Use. *Biol. Psychiatry* **94**, 888–897 (2023). doi: 10.1016/j.biopsych.2023.04.018; pmid: 37120062
41. D. W. Bayless *et al*., A neural circuit for male sexual behavior and reward. *Cell* **186**, 3862–3881.e28 (2023). doi: 10.1016/j.cell.2023.07.021; pmid: 37572660
42. S. M. Miller, J. S. Lonstein, Dopaminergic projections to the medial preoptic area of postpartum rats. *Neuroscience* **159**, 1384–1396 (2009). doi: 10.1016/j.neuroscience.2009.01.060; pmid: 19409227
43. S. X. Zhang *et al*., Hypothalamic dopamine neurons motivate mating through persistent cAMP signalling. *Nature* **597**, 245–249 (2021). doi: 10.1038/s41586-021-03845-0; pmid: 34433964
44. J. Kohl *et al*., Functional circuit architecture underlying parental behaviour. *Nature* **556**, 326–331 (2018). doi: 10.1038/s41586-018-0027-0; pmid: 29643503
45. G.-W. Zhang *et al*., Medial preoptic area antagonistically mediates stress-induced anxiety and parental behavior. *Nat. Neurosci.* **24**, 516–528 (2021). doi: 10.1038/s41593-020-00784-3; pmid: 33526942
46. K. Fukumitsu *et al*., Amylin-Calcitonin receptor signaling in the medial preoptic area mediates affiliative social behaviors in female mice. *Nat. Commun.* **13**, 709 (2022). doi: 10.1038/s41467-022-28131-z; pmid: 35136064
47. L. Mei, R. Yan, L. Yin, R. M. Sullivan, D. Lin, Antagonistic circuits mediating infanticide and maternal care in female mice. *Nature* **618**, 1006–1016 (2023). doi: 10.1038/s41586-023-06147-9; pmid: 37286598
48. S. C. Motta *et al*., Dissecting the brain's fear system reveals the hypothalamus is critical for responding in subordinate conspecific intruders. *Proc. Natl. Acad. Sci. U.S.A.* **106**, 4870–4875 (2009). doi: 10.1073/pnas.0900939106; pmid: 19273843
49. N. F. Parker *et al*., Reward and choice encoding in terminals of midbrain dopamine neurons depends on striatal target. *Nat. Neurosci.* **19**, 845–854 (2016). doi: 10.1038/nn.4287; pmid: 27110917
50. A. Mohebi *et al*., Dissociable dopamine dynamics for learning and motivation. *Nature* **570**, 65–70 (2019). doi: 10.1038/s41586-019-1235-y; pmid: 31118513
51. Q. Shan, Y. Hu, S. Chen, Y. Tian, Nucleus accumbens dichotomically controls social dominance in male mice. *Neuropsychopharmacology* **47**, 776–787 (2022). doi: 10.1038/s41386-021-01220-1; pmid: 34750567
52. G. D. Stuber, A. M. Stamatakis, P. A. Kantak, Considerations when using cre-driver rodent lines for studying ventral tegmental area circuitry. *Neuron* **85**, 439–445 (2015). doi: 10.1016/j.neuron.2014.12.034; pmid: 25611514
53. K. T. Beier *et al*., Topological Organization of Ventral Tegmental Area Connectivity Revealed by Viral-Genetic Dissection of Input-Output Relations. *Cell Rep.* **26**, 159–167.e6 (2019). doi: 10.1016/j.celrep.2018.12.040; pmid: 30605672
54. K. T. Beier *et al*., Circuit Architecture of VTA Dopamine Neurons Revealed by Systematic Input-Output Mapping. *Cell* **162**, 622–634 (2015). doi: 10.1016/j.cell.2015.07.015; pmid: 26232228
55. A. A. Grace, S. B. Floresco, Y. Goto, D. J. Lodge, Regulation of firing of dopaminergic neurons and control of goal-directed behaviors. *Trends Neurosci.* **30**, 220–227 (2007). doi: 10.1016/j.tins.2007.03.003; pmid: 17400299
56. D. Chaudhury *et al*., Rapid regulation of depression-related behaviours by control of midbrain dopamine neurons. *Nature* **493**, 532–536 (2013). doi: 10.1038/nature11713; pmid: 23235832
57. J. K. Dreyer, K. F. Herrik, R. W. Berg, J. D. Hounsgaard, Influence of phasic and tonic dopamine release on receptor activation. *J. Neurosci.* **30**, 14273–14283 (2010). doi: 10.1523/JNEUROSCI.1894-10.2010; pmid: 20962248
58. J. D. Berke, What does dopamine mean? *Nat. Neurosci.* **21**, 787–793 (2018). doi: 10.1038/s41593-018-0152-y; pmid: 29760524
59. S. Sarno *et al*., Dopamine firing plays a dual role in coding reward prediction errors and signaling motivation in a working memory task. *Proc. Natl. Acad. Sci. U.S.A.* **119**, e2113311119 (2022). doi: 10.1073/pnas.2113311119; pmid: 34992139
60. Y. Wang, O. Toyoshima, J. Kunimatsu, H. Yamada, M. Matsumoto, Tonic firing mode of midbrain dopamine neurons continuously tracks reward values changing moment-by-moment. *eLife* **10**, e63166 (2021). doi: 10.7554/eLife.63166; pmid: 33689680
61. A. C. Krok *et al*., Intrinsic dopamine and acetylcholine dynamics in the striatum of mice. *Nature* **621**, 543–549 (2023). doi: 10.1038/s41586-023-05995-9; pmid: 37558873
62. Q. Song *et al*., An ACC-VTA-ACC positive-feedback loop mediates the persistence of neuropathic pain and emotional consequences. *Nat. Neurosci.* **27**, 272–285 (2024). doi: 10.1038/s41593-023-01519-w; pmid: 38172439
63. C. Wang *et al*., Synaptotagmin-11 is a critical mediator of parkin-linked neurotoxicity and Parkinson's disease-like pathology. *Nat. Commun.* **9**, 81 (2018). doi: 10.1038/s41467-017-02593-y; pmid: 29311685
64. L. Wang *et al*., Cocaine induces locomotor sensitization through a dopamine-dependent VTA-mPFC-FrA cortico-cortical pathway in male mice. *Nat. Commun.* **14**, 1568 (2023). doi: 10.1038/s41467-023-37045-3; pmid: 36944634
65. L. Hunger, A. Kumar, R. Schmidt, Abundance Compensates Kinetics: Similar Effect of Dopamine Signals on D1 and D2 Receptor Populations. *J. Neurosci.* **40**, 2868–2881 (2020). doi: 10.1523/JNEUROSCI.1951-19.2019; pmid: 32071139
66. J. C. Martel, S. Gatti McArthur, Dopamine Receptor Subtypes, Physiology and Pharmacology: New Ligands and Concepts in Schizophrenia. *Front. Pharmacol.* **11**, 1003 (2020). doi: 10.3389/fphar.2020.01003; pmid: 32765257
67. A. Bedrov, S. L. Gable, Thriving together: The benefits of women's social ties for physical, psychological and relationship health. *Philos. Trans. R. Soc. London Ser. B* **378**, 20210441 (2023). doi: 10.1098/rstb.2021.0441; pmid: 36440568
68. A. J. Rose, K. D. Rudolph, A review of sex differences in peer relationship processes: Potential trade-offs for the emotional and behavioral development of girls and boys. *Psychol. Bull.* **132**, 98–131 (2006). doi: 10.1037/0033-2909.132.1.98; pmid: 16435959
69. S. Ayash *et al*., Fear circuit-based neurobehavioral signatures mirror resilience to chronic social stress in mouse. *Proc. Natl. Acad. Sci. U.S.A.* **120**, e2205576120 (2023). doi: 10.1073/pnas.2205576120; pmid: 37068238
70. Q. Song *et al*., Selective Phosphorylation of AMPA Receptor Contributes to the Network of Long-Term Potentiation in the Anterior Cingulate Cortex. *J. Neurosci.* **37**, 8534–8548 (2017). doi: 10.1523/JNEUROSCI.0925-17.2017; pmid: 28765333
71. P. C. Keyes *et al*., Orchestrating Opiate-Associated Memories in Thalamic Circuits. *Neuron* **107**, 1113–1123.e4 (2020). doi: 10.1016/j.neuron.2020.06.028; pmid: 32679036
72. S. Lin *et al*., Somatostatin-Positive Neurons in the Rostral Zona Incerta Modulate Innate Fear-Induced Defensive Response in Mice. *Neurosci. Bull.* **39**, 245–260 (2023). doi: 10.1007/s12264-022-00958-y; pmid: 36260252
73. X. Zhu *et al*., Distinct thalamocortical circuits underlie allodynia induced by tissue injury and by depression-like states. *Nat. Neurosci.* **24**, 542–553 (2021). doi: 10.1038/s41593-021-00811-x; pmid: 33686297
74. M. Li *et al*., Impaired D2 receptor-dependent dopaminergic transmission in prefrontal cortex of awake mouse model of Parkinson's disease. *Brain* **142**, 3099–3115 (2019). doi: 10.1093/brain/awz243; pmid: 31504219
75. B. Rein, K. Ma, Z. Yan, A standardized social preference protocol for measuring social deficits in mouse models of autism. *Nat. Protoc.* **15**, 3464–3477 (2020). doi: 10.1038/s41596-020-0382-9; pmid: 32895524

76. Z. Dong *et al*., CUL3 Deficiency Causes Social Deficits and Anxiety-like Behaviors by Impairing Excitation-Inhibition Balance through the Promotion of Cap-Dependent Translation. *Neuron* **105**, 475–490.e6 (2020). doi: 10.1016/j.neuron.2019.10.035; pmid: 31780330
77. P. Curzon, N. R. Rustay, K. E. Browman, in *Methods of Behavior Analysis in Neuroscience*, J. J. Buccafusco, Ed. (CRC Press/Taylor & Francis, 2009), pp. 19–37.

ACKNOWLEDGMENTS

We thank S. Qiu (Arizona State University, USA), B. Li (Sun Yat-Sen University, China), and W. Wang (The Fourth Military Medical University, China) for reading the manuscript; Y. Hao (Core Facilities Sharing Platform, Xi'an Jiaotong University, China) for assistance with confocal imaging; and E. Wang (High School Affiliated to Xi'an Jiaotong University, China) for artwork. **Funding:** This work was supported by the National Natural Science Foundation of China (32171233 and 31670843 to C.W., 81901308 to H.X., 81974203 to X.K., 32300819 to Y.C., 82030007 to C. Zhang, 32400650 to R.H., and 32000704 to Q.S.), the Natural Science Foundation of Shaanxi Province of China (2023-ZDLSF-23, 2021TD-37, and 2019JC-07 to C.W.; 2020JQ-029 to Q.S.; 2023-JC-QN-0236 to N.D.; 2024JC-YBMS-146 to H.X.; JC-YBQN-0172 to C. Zheng; and 2024JC-YBMS-141 and 2023SYJ09 to R.H.), the Sichuan Science and Technology Program (2022YFS0615 and 2024ZYD0077 to X.K.), the China Postdoctoral Science Foundation (2018M640972 to Q.S.; 2022M712543 to N.D.; and 2024M752559, 2024T170724, and GZC20232111 to Y.C.), the Shaanxi Postdoc Funding (2023BSHTBZZ15 to H.X., 2023BSHYDZZ39 to Y.C., and 2023BSHEDZZ67 to C.Zhe), and the Luzhou Science and technology Program (2024LZXNYDJ002 to X.K.). **Author contributions:** C.W., X.K., H.X., C.Zha., and A.W. conceived the study and designed the experiments with help of Q.Q. A.W., A.Z., C.Zhe., N.D., X.C., X.D., S.Z., X.L., J.J., Y.Q., Y.Y., Y.G., Bi.W., J.H., J.Y., W.L., K.H., Y.L., F.M., R.W., M.S., Bo.W., Y.Z., Y.C., Q.S., and R.H. performed the experiments and analyses. C.W., H.X., X.K., C.Zha., A.W., and N.G. wrote the manuscript. All authors reviewed the manuscript and approved its submission. **Competing interests:** The authors declare that they have no competing interests. There is no consultation, paid or unpaid, and related patent utilized or applied in or based on this work. **Data and materials availability:** The data that support the findings of this study are available in the main manuscript or the supplementary materials. Source data are provided with this paper.

SUPPLEMENTARY MATERIALS

science.org/doi/10.1126/science.adq7001
Figs. S1 to S12
MDAR Reproducibility Checklist

Submitted 27 May 2024; accepted 8 November 2024
10.1126/science.adq7001